

JGR Atmospheres

RESEARCH ARTICLE

10.1029/2020JD034174

Key Points:

- NO₂ columns from Tropospheric Monitoring Instrument (TROPOMI) are used to estimate NO_x production per flash
- Mean NO_x production by optically detected lightning flashes equals 175 ± 100 mol per flash for 29 case studies over the United States
- Mean NO_x production by radio-signal-detected lightning flashes equals 120 ± 65 mol per flash for 29 case studies over the United States

Correspondence to:




D. Allen,
djallen@umd.edu

Citation:

Allen, D., Pickering, K. E., Bucsel, E., Van Geffen, J., Lapiere, J., Koshak, W., & Eskes, H. (2021). Observations of lightning NO_x production from Tropospheric Monitoring Instrument case studies over the United States. *Journal of Geophysical Research: Atmospheres*, 126, e2020JD034174. <https://doi.org/10.1029/2020JD034174>

Received 30 OCT 2020
 Accepted 20 APR 2021

Observations of Lightning NO_x Production From Tropospheric Monitoring Instrument Case Studies Over the United States

Dale Allen¹ , Kenneth E. Pickering¹ , Eric Bucsel², Jos Van Geffen³ , Jeff Lapiere⁴ , William Koshak⁵, and Henk Eskes³

¹Department of Atmospheric and Oceanic Science, University of Maryland, College Park, MD, USA, ²SRI International, Menlo Park, CA, USA, ³Royal Netherlands Meteorological Institute, De Bilt, Netherlands, ⁴Earth Networks, Germantown, MD, USA, ⁵NASA Marshall Space Flight Center, Huntsville, AL, USA

Abstract Nitrogen oxides produced by lightning (LNO_x) play an important role in determining mid- and upper-tropospheric concentrations of the hydroxyl radical (OH), methane (CH₄), and ozone (O₃). The moles of NO_x produced per flash was examined using nitrogen dioxide (NO₂) columns and cloud properties from the Tropospheric Monitoring Instrument (TROPOMI) and flash counts from the Geostationary Lightning Mapper (GLM) aboard the Geostationary Operational Environmental Satellite-16 (GOES-16) and Earth Networks Total Lightning Network (ENTLN) for 29 convective systems over the United States that occurred during 2018 and 2019. For each of the case studies, the LNO_x production efficiency (PE) was estimated using TROPOMI pixels over deep convection. First, the NO_x columns associated with the TROPOMI NO₂ columns were estimated using a specially derived air mass factor (AMF). The tropospheric column due to recent lightning was then determined by subtracting from the median NO_x column a background representative of the NO_x column due to sources other than recent lightning. Then, the PE was calculated by multiplying the LNO_x column by the storm area and dividing by the number of flashes contributing to the column. For a three-hour chemical lifetime, the mean PE was found to be 175 ± 100 mol per flash for optical flashes from GLM and 120 ± 65 mol per flash for radio-wave-detected flashes from ENTLN. The uncertainty associated with these values is mostly due to uncertainties in tropospheric background, AMF, and detection efficiency. GLM PE for individual systems was found to be positively correlated with optical energy.

Plain Language Summary Lightning produces nitrogen oxides (NO_x) as the extreme temperatures within lightning channels break apart molecular nitrogen (N₂) and oxygen (O₂). NO_x produced by lightning (LNO_x) plays an important role in determining mid- and upper-tropospheric concentrations of the hydroxyl radical (OH), the atmosphere's cleanser; methane (CH₄), an especially potent greenhouse gas; and ozone (O₃), a greenhouse gas and pollutant. In this study, NO_x production per lightning flash was examined for 29 convective systems over the eastern- and central- United States that occurred during the warm seasons of 2018 and 2019 using nitrogen dioxide (NO₂) retrievals and cloud properties from the Tropospheric Monitoring Instrument (TROPOMI) aboard the Copernicus Sentinel-5 Precursor satellite and lightning flash counts from a satellite-based Geostationary Lightning Mapper (GLM) and the ground-based Earth Networks Total Lightning Network (ENTLN). The mean moles of NO_x produced per flash was found to equal ~180 moles per flash for optically detected flashes from GLM and ~120 moles per flash for radio-signal-detected flashes from ENTLN. These values are on the lower end of the commonly cited range of 100–500 moles per flash for midlatitude flashes.

1. Introduction

Nitrogen oxides (NO_x; nitric oxide [NO] + nitrogen dioxide [NO₂]) produced by lightning (LNO_x) via the Zel'dovich mechanism (Zel'dovich et al., 1947) are important contributors to tropospheric atmospheric composition and radiative forcing (Finney et al., 2018; Lacis et al., 1990; Liaskos et al., 2015; W. Wang et al., 1993).

We have previously used NO₂ columns from the Ozone Monitoring Instrument (OMI) to obtain estimates of LNO_x production per flash over the Gulf of Mexico (Pickering et al., 2016) and in convective events

during NASA's Tropical Composition, Cloud and Climate Coupling (TC4) field program based in Costa Rica (Bucsela et al., 2010). More recently we have conducted LNO_x analyses using OMI NO₂ and detection efficiency (DE) adjusted lightning flashes from the World Wide Lightning Location Network (WWLLN) over broad regions of the tropics (Allen et al., 2019) and midlatitudes (Bucsela et al., 2019) using a more refined algorithm. In the midlatitudes, we found that lightning flash counts from WWLLN were distinctly correlated with LNO_x estimates from OMI. The observations yielded a mean midlatitude production efficiency (PE) of 180 ± 100 moles of NO_x per flash. LNO_x production was found to decrease with flash rate, in agreement with literature that indicates shorter flash lengths and consequently lower PE per flash in high-flash rate storms (Bruning & MacGorman, 2013; Bruning & Thomas, 2015; Davis et al., 2019; Mecikalski et al., 2015; Zhang & Cummins, 2020). In the tropics, we found a mean LNO_x production of 170 ± 100 mol per flash with the mean PE at tropical marine locations with low flash rates approximately twice as large as at tropical continental locations with high flash rates. Recently, NO₂ columns from the NASA Goddard Geo-CAPE Airborne Simulator (GCAS) were used with flash counts from the ground-based Earth Networks Total Lightning Network (ENTLN) and Geostationary Lightning Mapper (GLM) aboard the Geostationary Operational Environmental Satellite-16 (GOES-16) hereafter referred to as GLM16 to estimate LNO_x PE for 10 convective systems observed over the U.S. and western Atlantic during the GOES-R Post Launch Test (GOES-R PLT) Field Campaign during spring 2017 (Allen et al., 2021; Padula et al., 2017). The mean PE for an assumed two-hour chemical lifetime was determined to be 360 ± 180 mol per flash for optically detected GLM flashes and 230 ± 115 mol per flash for radio-wave-detected Earth Networks Total Lightning Network (ENTLN) flashes. NO_x production per flash was found to be positively correlated with flash multiplicity and optical energy but negatively correlated with flash density.

In this study, NO_x production per lightning flash is estimated for 29 individual thunderstorm systems over the U.S. and western Atlantic during Summer 2018 and Spring/Summer 2019 using modified NO₂ columns from the Tropospheric Monitoring Instrument (TROPOMI) and flash rates from the satellite-based GLM16 and the ground-based ENTLN. The goal of this study is to provide an estimate of LNO_x PE and uncertainty derived from the much finer resolution of TROPOMI compared with OMI and the better defined DEs of GLM and ENTLN compared with WWLLN. The data sets used in this study are discussed in Section 2. The methodology is discussed in Section 3. Section 4 examines lightning flash counts and TROPOMI products for 5 selected cases. Section 5 discusses findings for the entire campaign, while Section 6 gives conclusions. Appendix A gives details on how TROPOMI products over deep convective scenes were processed. Appendix B gives a list of acronyms.

2. Data Sets

LNO_x PE is determined using tropospheric NO₂ columns and cloud properties from TROPOMI and flash counts from ENTLN and GLM16. These data sets are introduced in this section.

2.1. TROPOMI

TROPOMI (Veefkind et al., 2012) onboard the European Space Agency Copernicus Sentinel-5 Precursor satellite is a passive imaging spectrometer that retrieves numerous trace gases including NO₂ and cloud products such as cloud fraction and cloud top pressure. The retrieval of the tropospheric NO₂ vertical column density (VCD) is a three-step procedure: (1) slant column density (SCD) retrieval using differential optical absorption spectroscopy (DOAS), (2) determination and subtraction of the stratospheric component using output from a chemistry-and transport model and data assimilation, and (3) conversion of the tropospheric SCD into the VCD using a tropospheric air mass factor (AMF) (van Geffen et al., 2020). The horizontal resolution of the NO₂ and cloud products at nadir is ~ 3.6 km (cross track) \times 7.2 km (along-track) prior to August 6, 2019 and 3.6×5.6 km beginning August 6, 2019. The swath of TROPOMI is 2,600 km wide allowing for global coverage each day within our region of interest.

In this study, the production of NO_x by lightning is examined using TROPOMI NO₂ columns (V_{NO_2}) in/over deep convective pixels, which are defined as pixels with cloud top pressures of less than 500 hPa and effective cloud fractions in the NO₂ window greater than 0.95. See Section 3.1 of Allen et al. (2019) for a justification of the 500 hPa threshold. The cloud pressure is determined using the Fast Retrieval Scheme

for Clouds from the Oxygen A-band-S (FRESCO-S) algorithm, a high spectral resolution version of the FRESCO+ algorithm (P. Wang et al., 2008), using measurements in and around the O₂ A-band (760 nm). In theory, the cloud fraction and cloud radiance fraction could also be retrieved in the A-band; however, in practice, the cloud fraction is retrieved in the NO₂ window, centered at 440 nm, due primarily to a misalignment between ground pixel field-of-views of the visible and near-infrared bands (van Geffen et al., 2019). As of mid-2020, the operational retrieval algorithm for TROPOMI NO₂ is v1.3.2, which is based on v1.0 of the L1B TROPOMI retrieval system. However, most of the analysis in this study uses NO₂ version 2.1_test, a modified Copernicus Sentinel NO₂ data product, also based on v1.0 of L1B. It includes spike removal to better deal with saturation and blooming effects in the radiance spectra (Ludewig et al., 2020), which provides increased data coverage over bright (deep convective cloud) scenes relative to the current operational version. The quality assurance value (qa_value) is a standard TROPOMI data product (Eskes et al., 2019) that indicates the quality of NO₂ retrievals. In this study, retrievals with qa_values of 0.28–0.74 are used to estimate LNO_x PE. Retrievals with qa_values of 0.50–0.74 are deemed to be of good quality, while retrievals with qa_values of 0.28–0.49 are deemed to be of fair quality. The upper bound (0.74) is the maximum qa_value for retrievals over clouds. See Appendix A for a justification of the lower bound and also an examination of how the quality of V_{NO₂} retrievals over deep convection varies with qa_value.

2.2. ENTLN

The ENTLN is a lightning locating system that detects low frequency sferics (pulses) from cloud-to-ground (CG) and intracloud (IC) flashes using radio waves in the 1-Hz to 12-MHz range. Pulses are grouped into flashes using 10-km and 0.7-s proximity thresholds (Marchand et al., 2019). ENTLN metrics for individual flashes include time, location, type (CG or IC), peak current, and multiplicity (i.e., the number of pulses or strokes that compose each flash). In this study, the CG DE of ENTLN flashes is assumed to be 100% based on studies in Florida (Zhu et al., 2017) and New Mexico (Sonnenfeld et al., 2021). Technically, this value is biased high because no system will detect all flashes. However, 100% is reasonable given these studies and uncertainties in flash classification and false alarm rate (FAR). An IC DE of 90% is assumed based on a comparison of ENTLN flash counts with NASA Marshall Fly's Eye GLM Simulator (FEGS) (Quick et al., 2017) observations during the GOES-R PLT field campaign (Allen et al., 2021). Recently, Blakeslee et al. (2020) estimated the IC DE via comparison of ENTLN and International Space Station Lightning Imaging Sensor (ISS-LIS) flashes over the eastern two thirds of the U.S during the 2017–2019 time period. That analysis yielded a DE of 79 ± 18%, which is ~10% lower than the value used in this study. Thus, the ENTLN DEs used in this study are optimistic, which could lead to a small (likely <10%) underestimation of flashes and overestimation of PE.

2.3. GLM

The GLM is a near-infrared optical transient detector with a resolution of 8 km at nadir and 14 km at edge that images the Earth at 777 nm every 2 milliseconds (ms) allowing the distribution of lightning flashes to be mapped (Goodman et al., 2013; Rudlosky et al., 2019). Currently, GLM instruments aboard GOES-16 and GOES-17 are positioned at 75.2°W (GLM16) and 137.2°W (GLM17). In this study, data from GLM16 that was launched on November 19, 2016 and became operational in March 2017 is used. A GLM event is recorded when transient changes in pixel brightness exceed a threshold. After removing non-lightning artifacts, events are clustered using a Lightning Cluster and Filtering Algorithm (LCFA) that gathers events into groups and groups into flashes (Bitzer, 2017; Goodman et al., 2012; Mach, 2020). The latitude and longitude associated with each flash is obtained by weighting the latitudes and longitudes of constituent events by the optical energy of each event. Due to operational constraints, the total number of events per group and groups per flash is limited to 101 and flashes are limited to 3 s in length (Peterson, 2019). The artificial termination of flashes is a rare occurrence for storms with fewer than 40 flashes per second. However ~30% of the GLM flashes that occur in very high flashing storms were artificially terminated (Mach, 2020). These storms account for 2.5% of total flashes and have flash rates exceeding 64 flashes over a 90-s period. Thus, GLM flash rates in high flash rate storms may be biased high, resulting in a low-bias in LNO_x PE. An investigation of the magnitude of this bias is beyond the scope of this study as it would require a re-processed GLM16 data set with a modified LCFA.

Table 1
Sampling Details for the 29 Cases Examined During This analysis

#	Date	Lon range (°)	Lat range (°)	Storm region	Overpass time (UTC)	# GLM16 flashes	# ENLN flashes	GLM/ENLN
1	July 21, 2018	86–81	28–33	FL-GA-AL	1909	80,611	107,512	0.75
2	July 23	90–82	24–30	eGulf	1831	312,756	372,845	0.84
3	July 26	83–79	27.5–30.5	FL-wAtlantic	1916	34,709	40,278	0.86
4	April 4, 2019	98–84	28–36	MS-AR-LA	1851	218,496	233,047	0.94
5	April 13	100–88	28–38	LA-AR-TX	1922	292,015	302,988	0.96
6	April 22	98–88	38–48	IA-MN-WI	1813	33,214*	36,909	0.90
7	April 30	105–87	33–45	KS-MO-NE-IA	1903	117,729	179,907	0.65
8	May 5	86–78	25–31	FL-wGulf	1910	92,043	128,572	0.72
9	May 6	102–95	38–43	NE-KS	1851	13,738*	25,502	0.54
10	May 6	100–95	25–30	sTX; wGulf	1851	37,813	62,105	0.61
11	May 6	82–73	25–31	North Atlantic; FL	1851	14,811	20,925	0.71
12	May 10	98–91	25–30	western Gulf; sTX	1916	243,635	283,883	0.86
13	May 28	98–88	37–43	MO, IA	1838	78,760*	131,484	0.60
14	May 31	70–60	35–40	wAtl; east of DE	1741	65,968	102,648	0.64
15	June 8	90–78	25–35	FL, GA, AL, eGulf	1831	143,759	176,006	0.82
16	June 11	87–78	25–31	FL; eGulf	1916	22,609	34,716	0.65
17	June 22	102–96	40–46	SD-NE	1909	18,148*	28,023	0.65
18	June 23	98–88	33–38	AR-MO-OK-KS	1850	197,473	265,031	0.75
19	June 30	95–87	42–48	WI-MN-IA	1818	116,328*	326,215	0.36
20	July 5	99–92	36–41	KS-MO	1825	73,205	126,968	0.58
21	July 6	88–82	27–31	eGulf, FL, GA, AL	1806	42,513	59,309	0.72
22	July 8	105–98	45–50	ND	1909	17,614*	26,926	0.65
23	July 13	83–77	33–36	SC-NC	1915	40,076	61,691	0.65
24	July 16	96–92	41–45	IA-MN	1818	18,090*	33,698	0.54
25	July 16	94–88	31–36	MS-AR-LA	1818	47,535	68,584	0.69
26	July 22	92–84	34–38	TN-KY	1806	15,567	26,076	0.60
27	August 9	77–72	30–34	wAtlantic-SC	1728	50,808	65,267	0.78
28	August 14	92–82	28–33	FL-AL-MS-eGulf	1916	103,065	134,168	0.77
29	August 15	100–92	38–43	NE-IA-MO-KS	1857	25,044*	41,855	0.60

Note. In the “Storm Region” column, prefixes “w”, “e”, “s”, “n”, and “c” are used for western, eastern, southern, northern, and central, while U.S. states are identified using standard 2 letter abbreviations. GLM16 and ENTLN flash counts are adjusted for DE and summed over a 12-h period ending at the “overpass” time defined as the time that TROPOMI exited the region of interest. GLM16 flash counts for storm regions with centers poleward of 40°N assume a DE of 50% and are identified with asterisks. GLM16 flash counts equatorward of 40°N assume a DE of 75%.

In this study, the GLM16 DE was initially assumed to equal 75% based on a comparison of GLM16 flash counts with FECS observations during the GOES-R PLT field campaign (Allen et al., 2021). A 75% DE is also consistent with that found by Bateman and Mach (2020). However, it was found that the ratio of GLM16 to ENTLN flashes was systematically lower over the Upper Midwest and Great Plains where anomalous polarity storms with lower GLM DEs are more common (Fuchs & Rutledge, 2018; Rust et al., 2004; Rutledge et al., 2020). For example, Rutledge et al. found GLM16 DEs of 10%–35% relative to the Lightning Mapping Array (LMA) for an inverted polarity storm over Colorado during the GOES-R PLT Field Campaign. Allen et al. found a GLM16 DE of 55% relative to FECS for this same system. Thus, using a DE of 75% for all storms is not justified. Based on these studies, Figures 3 and 4 of Bateman and Mach (2020), and also the GOES-16 GLM Level 2 Product Performance Guide (Koshak et al., 2018), we use a DE of 50% for the eight storms with region centers that are poleward of 39.9°N and west of 90°W. Table 1 shows the dates and

locations of each of the 29 case studies as well as DE-adjusted counts of GLM16 and ENTLN flashes within the regions of interest for the 12-h period preceding the TROPOMI overpass. Overall, the ratio of GLM16 to ENTLN flashes equaled 0.73 with the ratios for individual storms ranging from 0.36 to 0.96. The GLM16 FAR over the region of interest was less than 5% (see Figures 5 and 6 of Bateman & Mach 2020) and is not adjusted for in this study.

3. Methodology

Case studies were selected over the southern and/or central U.S., Gulf of Mexico, and western Atlantic (110°–60°W and 25°–50°N) by comparing the spatial distributions of GLM16 flashes and v1.3 TROPOMI NO₂ columns after aggregating GLM16 flashes onto the footprints of TROPOMI pixels within this region. The screening time periods were June 28–July 31, 2018 and April 1–September 5, 2019. For this region, cases were chosen from days with nearly complete GLM16 temporal coverage, more than 20,000 GLM16 flashes between 1300 and 1900 UT, and TROPOMI overpass times between 1730 and 1930 UTC. Specifically, GLM16 temporal coverage was checked and only days with 5 or fewer missing 20-s data sets during the 12-h period preceding the TROPOMI overpass time were considered. Convective features (generally large-area storm systems) with plentiful flashes and enhanced NO₂ were chosen for case study analysis. Based on this screening, 29 case studies were selected.

For each of the storm regions (see Table 1), Equation 1 was used with deep convective v2.1_test TROPOMI pixels to estimate the mean moles of NO_x produced per flash.

$$PE = \left[V_{tropLNO_x} \times A \right] / \left[N_A \times F \right], \quad (1)$$

where $V_{tropLNO_x}$ is the tropospheric column of NO_x due to recent lightning (petamolec cm⁻²), A is storm area (cm²), N_A is Avogadro's number (6.022×10^{23} molec mol⁻¹), and F is the number of flashes contributing to the LNO_x column. A , the deep convective area, is calculated by summing the area of deep convective TROPOMI pixels within the storm region plus the area of TROPOMI pixels within the storm area with undefined cloud fractions. The latter term is added on to more accurately estimate the storm area because blooming effects occasionally make it impossible to estimate the cloud fraction over deep convective pixels (see Appendix A). F is calculated using Equation 2 where advective loss ($AdvL_i$), defined in Equation 3, is an estimate of the fraction of each flash advected out of the region and not sampled by TROPOMI.

$$F = \sum_N (1 - AdvL_i) \times F_i \exp\left(- (t_o - t_i) / \tau\right), \quad (2)$$

In Equation 2, N is the total number of GLM16 or ENTLN flashes within the storm-region during the 12-h period before the TROPOMI overpass time. A 12-h flash window is unusually long for this type of analysis; however, it was chosen to avoid an arbitrary cut-off and because for a 3-h lifetime, 20% of the LNO_x signal remains after 5-h. F_i is the flash count assigned to an individual flash after adjusting for DE. Therefore, F_i would equal 1.33 flashes for a GLM16 flash with a DE of 0.75. The exponential term accounts for the relatively short lifetime of NO_x in the near field of convection. It includes t_o defined as the time of the TROPOMI overpass (hours) shown in Table 1, t_i defined as the time flash i occurred (hours), and τ , the assumed chemical lifetime of NO_x in the near field of convection (hours). Thus, the age of flashes relative to the TROPOMI overpass time is given by $(t_o - t_i)$. The choice of τ is critical because it determines the attenuation rate of NO₂, which also applies to lightning generated NO₂. The value of τ , 3 h, is taken from Nault et al. (2016, 2017) who found that the lifetime of lightning-generated NO_x in the near field of convection is 2–12 h depending on the proximity to convection. A three-hour lifetime is used in this study because of the close proximity to convection. However, sensitivity simulations were run for $\tau = 2$ –6 h.

$$AdvL_i = (t_o - t_i) \times (V_{200} \times \sin(\theta) / Hyp), \quad (3)$$

In Equation 3, the definitions of t_o and t_i are unchanged, but the units are seconds, V_{200} is the mean 200 hPa wind speed (m/s) at 18 UTC from Version 2 of the Modern-Era Retrospective analysis for Research and

Applications (MERRA-2) within the sampling region, θ (radians) is the difference in direction between the 200 hPa MERRA-2 winds and the storm direction, and Hyp (m) is the hypotenuse of the sampling region shown in Table 1. The storm direction is defined as the angle whose tangent is equal to $-dy/-dx$ where dx and dy are the east-west and north-south differences in mean location of GLM16 or ENTLN flashes between early and late in the flash counting window. In this study, the initial location is obtained by averaging the locations of the earliest one third flashes during the flash window while the final location is obtained by taking the mean of the locations of the latest one third of flashes.

$V_{tropLNOx}$, the NO_x column due to recent lightning, is determined using Equation 4. $V_{tropNOx}$, the tropospheric NO_x column, which is needed in Equation 4 is estimated using Equation 5.

$$V_{tropLNOx} = \text{Median}(V_{tropNOx}) - V_{tropbkgn}, \quad (4)$$

$$V_{tropNOx} = \left[S_{NO_2} - \text{Avg}(V_{stratNO_2} \times AMF_{strat}) \right] / AMF_{LNOx}, \quad (5)$$

where S_{NO_2} is the SCD of NO_2 , $V_{stratNO_2}$ is the stratospheric VCD of NO_2 , and AMF_{strat} is the stratospheric AMF. These three terms are standard TROPOMI output products. The portion of Equation 5 in square brackets is the tropospheric SCD of NO_2 . This term is obtained by subtracting the mean stratospheric SCD of NO_2 for deep convective pixels over the region of interest from the local value of S_{NO_2} . The mean stratospheric SCD of NO_2 is obtained by multiplying the VCD of NO_2 by the stratospheric air mass factor (AMF_{strat}) and averaging. The tropospheric SCD of NO_2 could also be estimated by multiplying the tropospheric VCD of NO_2 , V_{tropNO_2} , by the tropospheric AMF, AMF_{trop} (see Equation 6). These terms are also standard TROPOMI products.

$$V_{tropNOx} = \left[V_{tropNO_2} \times AMF_{trop} \right] / AMF_{LNOx} \quad (6)$$

However, Equation 5 is used in this study because versions 1.1 and 1.2 of the TROPOMI NO_2 product were often missing values for V_{tropNO_2} and sometimes missing values for $V_{stratNO_2}$ and AMF_{strat} in regions affected by deep convection and lightning. The use of Equation 5 increased the number of pixels available to estimate $V_{tropLNOx}$ and allowed for more robust estimates of PE. AMF_{LNOx} is a specially derived AMF that converts the tropospheric SCD of NO_2 to a VCD of LNO_x . It can be computed using TROPOMI cloud information and NO_2 and NO_x profiles representative of flashing storms from the NASA Global Modeling Initiative (GMI) model (Allen et al., 2010, 2019; Bucselo et al., 2019) or from cloud-scale simulations described in Ott et al. (2010). Profiles from the GMI model are based on the differences in simulations with and without the lightning source. Figure 1 shows area-mean values of AMF_{LNOx} for each of the 29 cases. The mean value of AMF_{LNOx} equals 0.41 ± 0.10 for GMI profiles and 0.32 ± 0.09 for Ott profiles. The Ott AMFs are smaller because they assume a larger portion of the column is in the upper troposphere where NO_2/NO_x ratios are smaller. On average, the use of Ott profiles increases $V_{tropNOx}$ and consequently PE by 31%. AMF_{LNOx} values for individual storms vary by approximately a factor of 2.5 from 0.19 to 0.51 for Ott and 0.25 to 0.62 for GMI.

$V_{tropLNOx}$ is calculated by subtracting a tropospheric background, $V_{tropbkgn}$, from the median value of $V_{tropNOx}$ calculated from deep convective pixels (both flashing and non-flashing) within the storm region with qa_{-} values of 0.28 or greater (see Equation 4). $V_{tropbkgn}$ is an estimate of the mean NO_x column of deep convective pixels within the region of interest that are minimally affected by recent lightning. $V_{tropbkgn}$ is a major source of uncertainty. Its lower (upper) bound is assumed to be given by the 10th (30th) percentile of the $V_{tropNOx}$ distribution obtained from non-flashing deep convective pixels. Pixels are considered to be non-flashing if they have less than one-flash during the 12-h period preceding the TROPOMI overpass after application of a boxcar smoother whose width equals 7×3 prior to August 6, 2019 and 7×5 on-and-after August 6, 2019. The along-track width of the smoother was changed on the sixth because the along-track TROPOMI pixel size changed from 7.2 to 5.6 km on that date. For comparison purposes, $V_{tropLNOx}$ is also calculated assuming a tropospheric background of 0 petamolec cm^{-2} . The latter option does not always result in the largest values of $V_{tropLNOx}$ as the 30th percentile of $V_{tropNOx}$ over non-flashing pixels is occasionally negative over unpolluted regions.

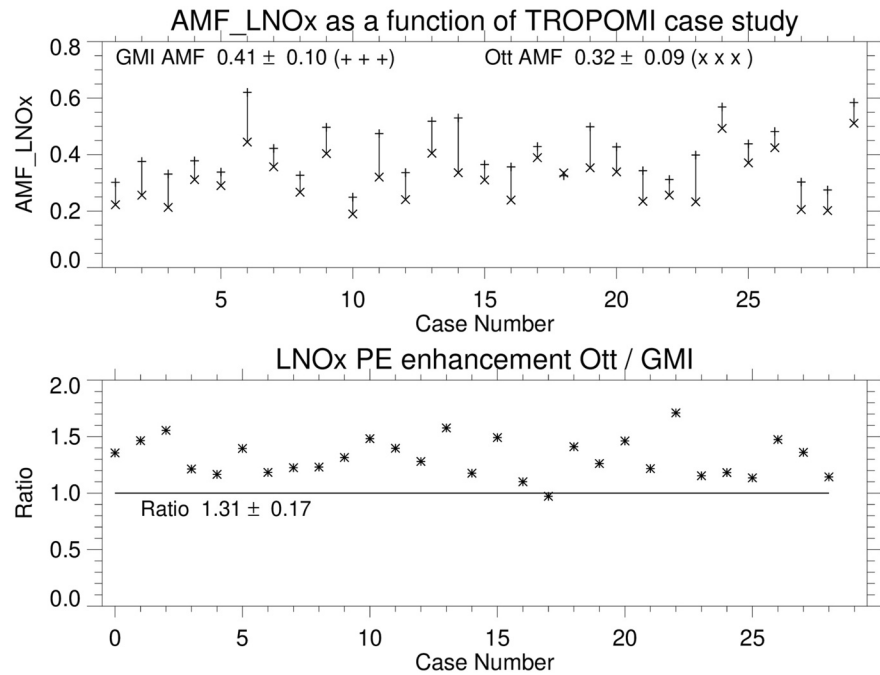


Figure 1. Time series showing case-to-case variability in AMF_{LNOx} for GMI profiles (+ + +) and Ott et al. profiles (x x x) (top figure). The bottom figure shows the enhancement in PE (inverse of GMI to Ott ratio) when the GMI profile is replaced by the Ott et al. profile.

The 10th percentile of the non-flashing $V_{tropNOx}$ distribution is chosen as a lower limit on the upper tropospheric background based on an analysis of data from the CRYSTAL-FACE (Cirrus Regional Study of Tropical Anvils and Cirrus Layers—Florida Area Cirrus Experiment) (Ridley et al., 2004) and GOES-R PLT field campaigns. During CRYSTAL-FACE, background NO amounts were typically 100–300 pptv between 10 km and the tropopause while storm anvil values exceeded 3,000 pptv over broad horizontal regions. During the GOES-R PLT, the ER-2 repeatedly crossed southern Louisiana, Mississippi, and Alabama alternately sampling locations with near-background and LNO_x-influenced columns. Differences in GCAS-based V_{tropNO_2} between these locations was consistent with a 5th percentile background. The background in this study is likely larger than the 5th percentile of $V_{tropNOx}$ because the spatial resolution of TROPOMI is coarser than that of GCAS and TROPOMI is a passive observer while the ER-2 flight track was chosen to sample both background and LNO_x-influenced air masses. The 30th percentile is chosen as an upper limit on the background based on an analysis of CRYSTAL-FACE and Deep Convective Clouds and Chemistry (DC3) measurements (Pickering et al., 2016). During CRYSTAL-FACE there were some cases where upwind storms contributed 1,000 pptv or more NO in the vicinities of sampled anvils, implying a >30% background. During DC-3, on one flight over the Gulf of Mexico, the background averaged ~33% of the mean value of the LNO_x outflow. Bucsela et al. (2019) obtained a mean midlatitude background of 55% for a gridded $1^\circ \times 1^\circ$ analysis using WWLLN flashes and OMI NO₂. However, on-going gridded analyses with GLM flashes and TROPOMI NO₂ indicates a lower background suggesting that noise in the WWLLN flashes and the coarse spatial resolution of OMI resulted in an overestimation of the background at TROPOMI pixel scales.

4. Selected Case Studies

In this section, the spatial distribution of GLM16 and ENTLN flashes and TROPOMI products is examined for five of the case studies. To focus on flashes that contribute the most to the TROPOMI signal, flash totals are shown for the five-hour period preceding the TROPOMI overpass time.

Figure 2 shows the spatial distribution of flashes and TROPOMI products on July 21, 2018 for a convective system centered over the panhandle of Florida and southern Georgia. The GLM16 recorded 50,123 flashes and ENTLN recorded 82,861 flashes mostly over the northwestern portion of the sampling region (28° –

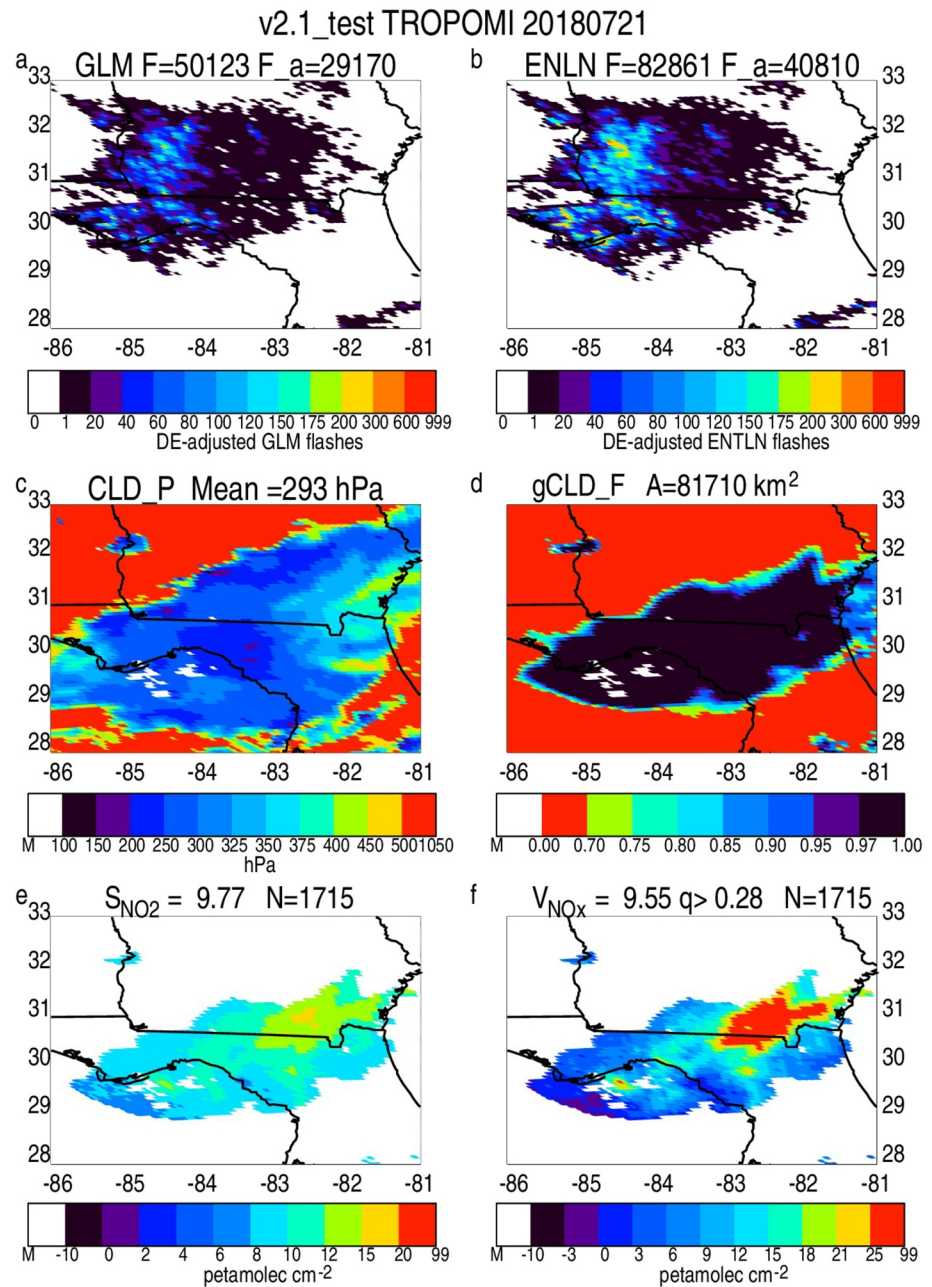


Figure 2. Lightning flash counts and Tropospheric Monitoring Instrument (TROPOMI) products for a deep convective system observed over the panhandle of Florida and southwest Georgia on July 21, 2018. (a) GLM16 flashes in each TROPOMI pixel during the 5-h period prior to the TROPOMI overpass, (b) Earth Networks Total Lightning Network (ENTLN) flashes in each TROPOMI pixel during same time period, (c) cloud pressure (hPa), (d) effective cloud fraction in the NO_2 window, (e) S_{NO_2} over deep convective pixels (petamolec cm^{-2}), and (f) V_{TropNO_x} over deep convective pixels (petamolec cm^{-2}). nF gives the number of flashes recorded during this 5-h period while nF_a gives the adjusted flash total that is used when estimating the PE; it includes adjustments for DE and the chemical lifetime of NO_x . The titles to Figures c–f also include information on the mean cloud top pressure, area of the deep convective region, mean S_{NO_2} and mean V_{TropNO_x} , respectively. The number of pixels with valid data (N) are also shown in Figures e–f.

33°N, 86°–81°W) between 1409 and the 1909 UTC overpass time (Figures 2a and 2b). The mean age of the flashes at the overpass time was ~ 2.7 h. After adjusting for DE and chemical lifetime, F was found to equal 29,170 flashes for GLM16 and 40,810 flashes for ENTLN. The deep convective region was determined using the cloud pressures and cloud fractions associated with this system (Figures 2c and 2d). The deep convective

region extends to the east and south of the flash region likely because mean upper tropospheric (200 hPa) winds at 18 UTC for this region as estimated by the MERRA-2 reanalysis (Gelaro et al., 2017) were from the west-northwest (292°) at 12 m s^{-1} while the GLM16 lightning centroid associated with this system moved mostly to the south (352°) between 1409 and 1909 UTC. NO_2 slant columns (S_{NO_2}) over deep convective pixels are shown in Figure 2e, while V_{tropNO_x} over deep convective pixels with $qa_values \geq 0.28$ are shown in Figure 2f. In general, columns are larger on the northeastern edge of the deep convective system. The spatial coverage of v2.1_test TROPOMI data was excellent for this case. The cloud fraction, pressure, and slant column (S_{NO_2}) were defined for 98% of the region with 86% of the pixels being good quality ($qa_value \geq 0.50$) and nearly all being of fair or good quality ($qa_value \geq 0.28$). The median column over good-quality pixels was $8.84 \text{ petamolec cm}^{-2}$ (not shown) while the median column over fair/good pixels was $9.55 \text{ petamolec cm}^{-2}$. The mean PE for this system was 312 mol per flash for GLM16 and 226 mol per flash for ENTLN where the means were obtained by averaging the median values over background type (10th or 30th percentile) and profile type (GMI or Ott). Relatively low AMFs of 0.30 for GMI and 0.22 for Ott contributed to the relatively high PE for this system.

Figure 3 shows the spatial distribution of flashes and TROPOMI products on May 6, 2019 over southern Texas. GLM16 recorded 17,707 flashes while ENTLN recorded 35,528 flashes within the sampling region ($25^\circ\text{--}30^\circ\text{N}$, $100^\circ\text{--}95^\circ\text{W}$) between 1351 and 1851 UTC (Figures 3a and 3b). The mean age of the flashes at the overpass time was $\sim 2.2 \text{ h}$. The upper tropospheric winds associated with this system as estimated by MERRA-2 were blowing from the southwest to northeast (230°) at 19 m s^{-1} while the cell itself moved to the east-northeast at 252° . Thus, the convective core of the system, as estimated using TROPOMI cloud top pressures (Figure 3c), was displaced to the northeast of the flashes. The cloud fraction, pressure, and slant column were defined for 97% of the pixels within the region with 85% of the deep convective pixels being of good quality and nearly all of fair/good quality. S_{NO_2} and especially V_{tropNO_x} were enhanced on the southwestern edge of the deep convective region (Figures 3e and 3f). The median column over good-quality pixels ($4.92 \text{ petamolec cm}^{-2}$) was higher than the median column over fair/good quality pixels ($4.59 \text{ petamolec cm}^{-2}$). The mean PE for this system was 586 mol per flash for GLM16 and 352 mol per flash for ENTLN. The high PE is partially due to the GMI AMF_{LNO_x} of 0.25 and Ott AMF_{LNO_x} of 0.19 for this system.

Figure 4 shows the spatial distribution of flashes and TROPOMI products on July 8, 2019 for a relatively isolated system over central North Dakota that was ongoing when TROPOMI sampling occurred; the mean age of GLM16 flashes associated with this system was only 20 min. The GLM16 recorded 2,234 flashes while ENTLN recorded 8,743 flashes within the sampling region ($45^\circ\text{--}50^\circ\text{N}$, $105^\circ\text{--}98^\circ\text{W}$) between 1409 and 1909 UTC (Figures 4a and 4b). The flash counts were adjusted to 4,011 flashes for GLM16 and 8,532 for ENTLN after adjusting for DE and flash age. For this northern storm, the GLM16 DE was assumed to be 50%. The upper tropospheric winds associated with this system were blowing from the southwest to northeast (232°) at a robust 33 m s^{-1} ; however, the narrow convective core of the system (Figures 4c and 4d) was displaced only slightly to the northeast due to the short time period between when the flashes occurred and when the storm was sampled. The cloud fraction, pressure, and slant column were defined for 98% of the deep-convective pixels within the region although only 16% of the pixels were of good quality likely due to low tropospheric AMFs due to the ongoing convection (see Appendix A). S_{NO_2} (Figure 4e) and V_{tropNO_x} (Figure 4f) were enhanced in the western edge of the deep convective region near the region of maximum flashes. The median column over the few good-quality pixels ($0.34 \text{ petamolec cm}^{-2}$) was much lower than the median column over fair/good quality pixels ($1.59 \text{ petamolec cm}^{-2}$). The mean PE was 171 mol per flash for GLM16 and 84 mol per flash for ENTLN. AMF_{LNO_x} values were 0.31 assuming a GMI profile and 0.26 assuming an Ott profile. These AMF_{LNO_x} values are 15%–20% below average.

Figure 5 shows the spatial distribution of flashes and TROPOMI products on August 9, 2019 for an isolated system over the South Atlantic Bight to the east of South Carolina ($30^\circ\text{--}34^\circ\text{N}$, $77^\circ\text{--}72^\circ\text{W}$); the mean age of flashes associated with this system was 1.66 h. The GLM16 recorded 10,870 flashes while ENTLN recorded 17,616 flashes within the sampling region between 1228 and 1728 UTC (Figures 5a and 5b). The flash counts were adjusted to 8,775 and 11,455 after adjusting for DE and flash age. The upper tropospheric winds associated with this system were blowing from the west-northwest to east-southeast (300°) at 16 m s^{-1} . The convective core of the system (Figures 5c and 5d) was aligned from east to west. GLM16 lightning data indicated that it moved to the west over the time period of interest. The cloud fraction, pressure, and slant

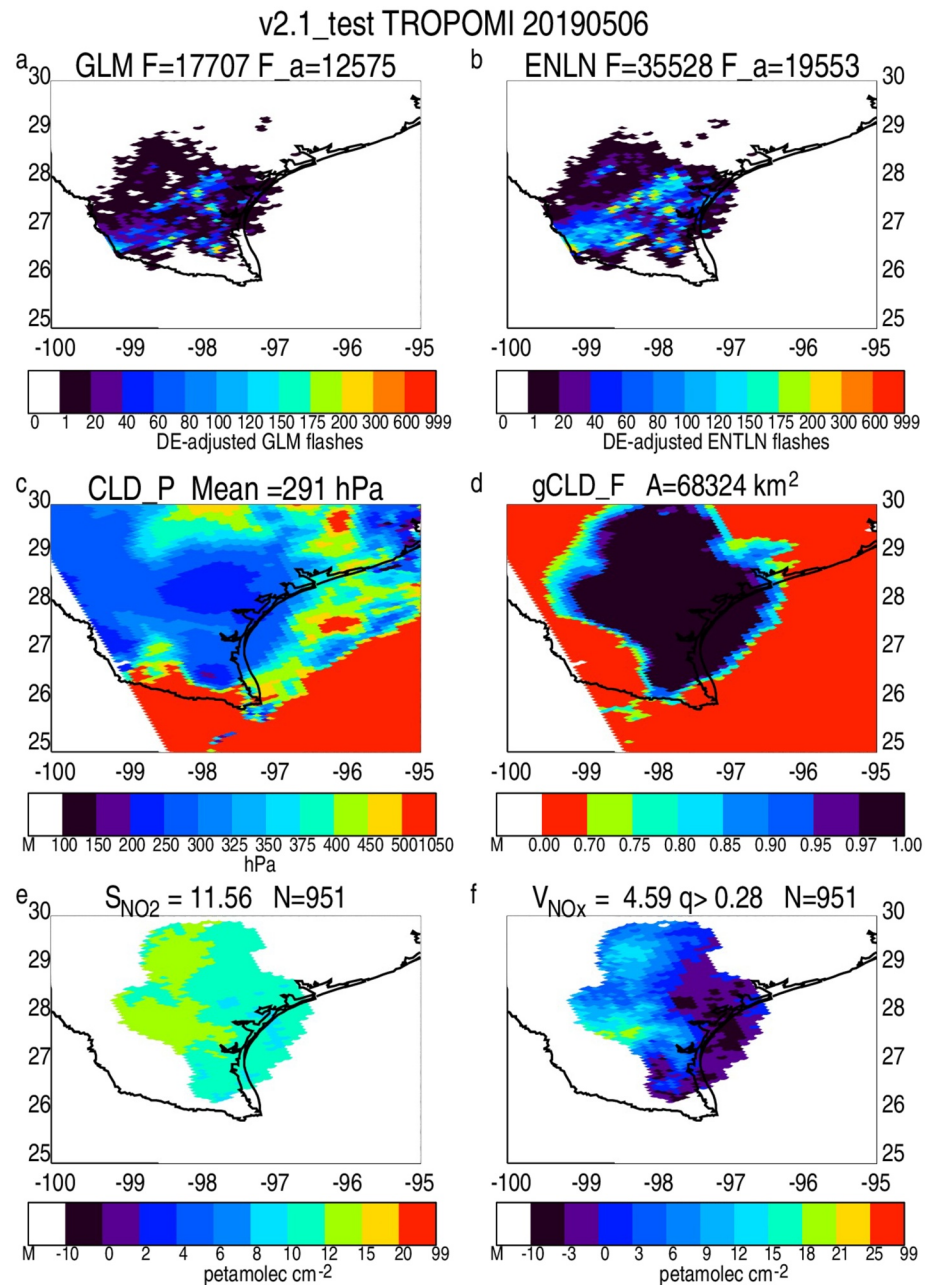


Figure 3. Same as Figure 2 but for deep convective system observed over southern Texas on May 6, 2019.

column were defined for all of the deep-convective pixels within the region of interest with 77% of the pixels being of good quality. S_{NO_2} (Figure 5e) was enhanced over two regions. The eastern region with cloud top pressures between 300 and 400 hPa had good quality pixels while the western region with cloud top pressures of ~ 200 hPa and high flash counts had fair quality retrievals likely due to the tropospheric AMF being less than one-tenth of the geometric AMF (see Appendix A). The median column over good-quality pixels (4.18 petamolec cm^{-2}) was lower than the median column over fair good quality pixels (4.82 petamolec cm^{-2}). The mean PE was 248 mol per flash for GLM16 and 192 mol per flash for ENTLN. AMF_{LNO_x} for this system was a relatively low 0.30 for a GMI profile and 0.21 for an Ott profile.

The final case to be highlighted occurred on August 15, 2019 near the border of Nebraska, Kansas, Iowa, and Missouri (38° – 43° N, 100° – 92° W). GLM16 recorded 10,081 flashes while ENTLN recorded 30,371 flashes.

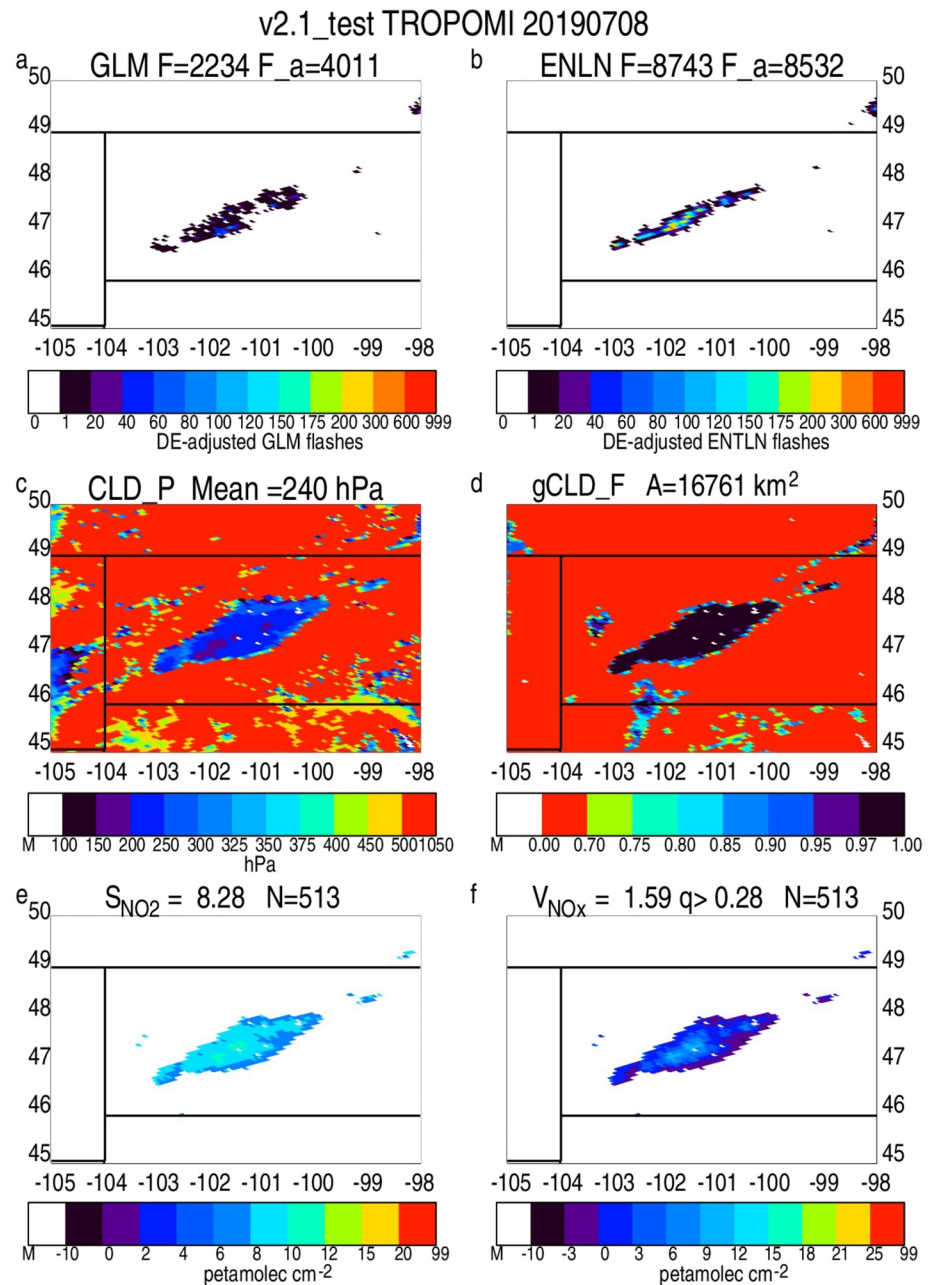


Figure 4. Same as Figure 2 but for a deep convective system observed over North Dakota on July 8, 2019.

The large discrepancy indicates that the GLM16 DE was unusually low perhaps due to the storm being anomalous in polarity and thus having a higher-than-normal percentage of low-altitude and/or short-duration flashes (Zhang & Cummins, 2020). Alternatively, GLM16 flash DE is also found to be low for severe (e.g., hail-producing) storms or storms with deep liquid water path regardless of polarity structure (Section 3.2 of Koshak et al., 2018). After adjusting for chemical lifetime and DE assuming a GLM16 DE of 50% and an ENTLN IC DE of 90% the GLM16 flash count was reduced to 8,524 while the ENTLN flash count was reduced by almost a factor of 2 to 15,508. The flashes associated with this storm (Figures 6a and 6b) were relatively old, the mean GLM16 age was 2.9 h while the mean ENTLN age was 2.6 h. The upper tropospheric winds associated with this system were blowing from the west-northwest to east-southeast (287°) at 31 m s⁻¹. GLM16 and ENTLN lightning data indicated that the convective core of the system as measured by the movement of the lightning centroid was moving in the same direction as the upper tropospheric winds

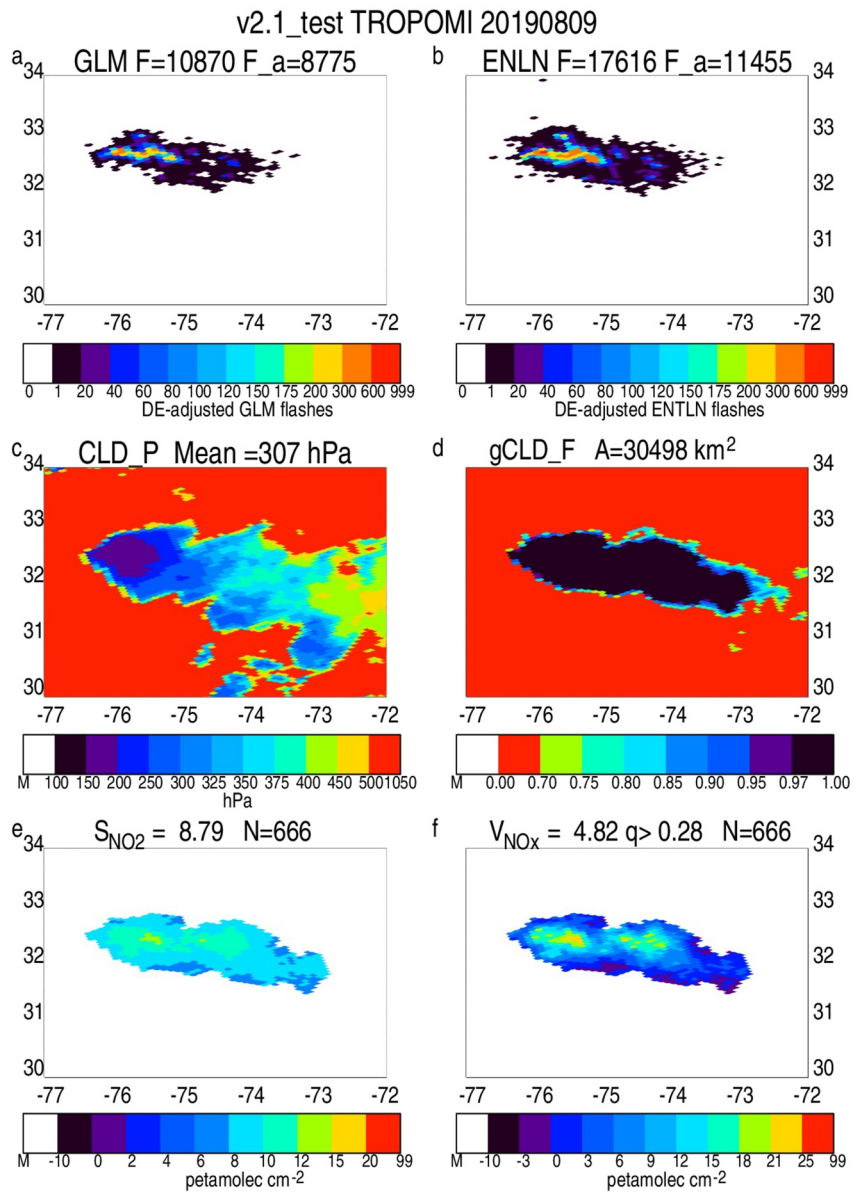


Figure 5. Same as Figure 2 but for a deep convective system observed over the South Atlantic Bight to the east of South Carolina on August 9, 2019.

(284° for ENLNL and 281° for GLM16). The cloud pressure, fraction, and slant column (Figures 6c–6e) were defined for 99% of the deep-convective pixels within the region; however, only 1% of the deep convective pixels had good quality NO₂ retrievals. Thus, LNO_x PE estimation for this storm is only possible when fair quality pixels are also included. S_{NO2} (Figure 6e) was enhanced over the western portion of the deep convective region. The median column over the few good-quality pixels (2.17 petamolec cm⁻²) was lower than the median column over fair/good quality pixels (2.95 petamolec cm⁻²). The mean PE was 186 mol per flash for GLM16 and 108 mol per flash for ENLNL. The AMF for this system was an unusually high 0.51 limiting the PE.

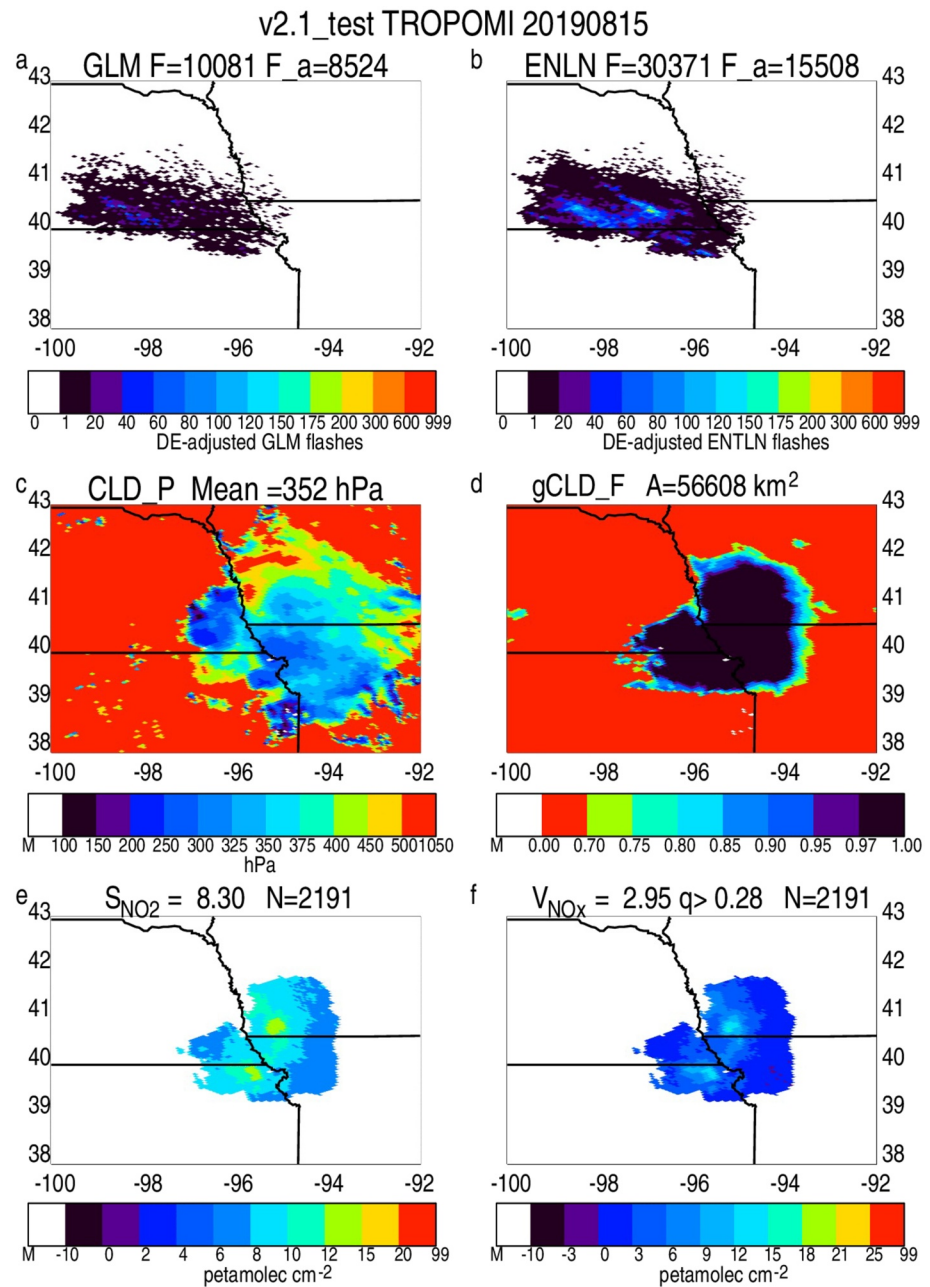


Figure 6. Same as Figure 2 but for a deep convective system observed over the north central U.S. on August 15, 2019.

5. Discussion

Table 2 shows storm-to-storm variations in TROPOMI products and LNO_x PE. The $Q > 50$ column shows the percent of pixels with q_a value > 0.5 . The mean is 57% with values for individual storms ranging from 1% to 100%. The variability is large because TROPOMI is sampling active thunderstorms with bright scenes with low values of AMF_{trop} in some cases and storm outflow in others. The mean V_{tropNO_x} is 4.4 ± 3.7 petamolec cm⁻² and the mean $V_{tropLNO_x}$ equals 3.0 ± 0.5 petamolec cm⁻². The variability of $V_{tropLNO_x}$ is much less than that of V_{tropNO_x} because $V_{tropbkgn}$ is sampled from a similar distribution as V_{tropNO_x} . Thus, relatively large values of $V_{tropbkgn}$ are accompanied by relatively large values of V_{tropNO_x} and vice versa. The Adv_Adjust column shows the adjustment applied to PE to account for advective loss. It has a mean of 1.16 ± 0.16 but ranges from 1.01 to 1.70. High values are associated with strong upper tropospheric winds, relatively old

Table 2
Statistics for the 29 Case studies

#	Date	Storm region	$Q > 0.50$	V_{tropNO_x}	V_{tropLNO_x}	Adv_Adjust	PE _{GLM16}	PE _{ENTLN}
			%	Peta molec cm ⁻²			Mol flash ⁻¹	
1	July 21, 2018	FL-GA-AL	86	9.6	6.3	1.15	312	226
2	July 23	Eastern Gulf	89	15.4	11.6	1.06	285	238
3	July 26	FL-wAtl	33	5.1	1.1	1.07	28	25
4	April 4, 2019	MS-AR-LA	51	6.7	1.8	1.04	187	154
5	April 13	LA-AR-TX	40	11.6	4.1	1.17	221	229
6	April 22	IA-MN-WI	62	1.7	1.8	1.26	244	278
7	April 30	KS-MO-NE-IA	21	5.5	2.9	1.04	397	234
8	May 5	FL-wGulf	63	5.4	7.9	1.01	179	125
9	May 6	NE-KS	59	1.4	0.9	1.25	202	75
10	May 6	sTX; wGulf	85	4.6	5.1	1.25	586	352
11	May 6	NAtl; central FL	68	-0.5	2.7	1.06	295	198
12	May 10	wGulf; sTX	98	11.7	3.4	1.31	160	127
13	May 28	MO, IA	5	2.1	2.2	1.25	211	130
14	May 31	wAtl; east of DE	100	5.8	3.8	1.10	210	137
15	June 8	FL, GA, AL, eGulf	94	3.2	1.6	1.04	73	52
16	June 11	FL; eGulf	46	-0.3	3.2	1.02	183	111
17	June 22	SD-NE	63	0.2	1.2	1.71	174	142
18	June 23	AR-MO-OK-KS	86	1.7	0.9	1.15	108	66
19	June 30	WI-MN-IA	2	3.8	3.0	1.20	364	133
20	July 5	KS-MO	53	0.3	1.8	1.11	223	144
21	July 6	eGulf, FL, GA, AL	72	2.8	2.0	1.01	37	194
22	July 8	North Dakota	16	1.6	2.3	1.19	171	84
23	July 13	SC-NC	29	3.4	2.7	1.03	81	57
24	July 16	IA-MN	44	5.1	1.2	1.55	165	50
25	July 16	MS-AR-LA	90	3.9	3.7	1.21	461	256
26	July 22	TN-KY	55	4.2	1.7	1.06	220	128
27	August 9	wAtlantic-SC	77	4.8	4.0	1.27	248	192
28	August 14	FL-AL-MS-eGulf	53	4.1	4.1	1.02	132	100
29	August 15	NE-IA-MO-KS	1	2.9	1.8	1.04	186	108
	Mean		57	4.4	3.0	1.16	219	150

Note: The “ $Q > 0.50$ ” column shows the percent of pixels with qa_value exceeding 0.5. The values vary widely thus the remaining columns show values of TROPOMI products for a qa_value minimum threshold of 0.28. The fifth and sixth columns show mean values of V_{tropNO_x} and V_{tropLNO_x} . The mean value of V_{tropLNO_x} varies with background type, flash source, and profile choice. The values shown were obtained by averaging these 8 values. The “Adv_Adjust” column shows the mean fractional increase in PE after adjusting for advective loss during the 12-h flash window. The final two columns show the GLM16 and ENTLN PE for each of the cases. The values have been adjusted for chemical-decay and advective loss and are averaged over 2 background options (10th and 30th percentile) and two profile types (GMI and Ott).

flashes, small areas of interest, and/or systems with a mismatch between storm movement and the direction of outflow (see Equation 3). The final two columns show GLM16 and ENTLN PE values for individual systems assuming a 3-h chemical lifetime and adjusting for detection-efficiency and advective loss. The PE values were obtained by averaging the values for two tropospheric backgrounds and two assumed profiles. The mean values are 219 ± 124 mol per flash for GLM16 and 150 ± 80 mol per flash for ENTLN. The PE values for individual systems range from 25 to 28 mol per flash for a July 26, 2018 storm over Florida to 352–586 mol per flash for the May 6, 2019 storm shown in Figure 3.

Table 3
LNO_x PE (Mean of the 29 Case Studies ± One Sigma) Assuming a 3-H Chemical Lifetime as a Function of TROPOMI Version (v1.3 or v2.1_test), Lightning Source (GMI or ENTLN), Profile Source (GMI or Ott), and Tropospheric Background Option (No Background (b00), 10th Percentile Background (b10), or 30th Percentile Background (b30))

	V1.3				V2.1_test			
	GLM16		ENTLN		GLM16		ENTLN	
	GMI	Ott	GMI	Ott	GMI	Ott	GMI	Ott
Q28 b00	205±160	259±190	134 ±110	171 ±133	236±185	298±219	156±136	199±163
	232 ± 175		153 ± 121		267 ± 202		178 ± 150	
Q28 b30	125±91	162±118	83 ±49	109 ±65	148±99	191±128	99±56	130±74
Q28 b10	202±108	264±141	133 ±72	174 ±96	233±117	302±150	160±82	209±109
	188 ± 114		124± 70		219 ± 124		150 ± 80	
Bias and uncertainty adjusted PE					175 ± 100		120 ± 65	

Note: The method used to determine the “Bias and uncertainty adjusted PE” values shown in the lower right is discussed in Section 5.2. Values for individual cases are calculated using pixels with qa_value ≥ 0.28.

5.1. Analysis of Variability

Table 3 shows variations in mean LNO_x PE for τ = 3 h as a function of TROPOMI version (V1.3 or V2.1_test), lightning source (GLM16 or ENTLN), profile type (GMI or Ott), and tropospheric background choice (b00 [no background], b30 [30th percentile background], and b10 [10th percentile background]). The PE for optically detected GLM16 flashes (219 mol per flash) is ~46% greater than the PE for radio-wave-detected ENTLN flashes (150 mol per flash) because GLM is unable to detect some smaller/weaker flashes detected by ENTLN. ENTLN and GLM use different lightning-observing techniques. ENTLN detects low frequency sferics, while GLM detects optical emissions of lightning from near the cloud top. As a result, ENTLN has more flashes. The 46% difference in PE between optically and radio-wave detected flashes in this study is a bit smaller than the 56% found by Allen et al. (2021) during the GOES-R PLT field campaign.

The 16%–18% increase in PE between v1.3 and v2.1_test is mostly due to a ~24% increase in the deep convective area, A, between v1.3 and 2.1_test. The increase in A is due to an increase in the number of deep convective pixels with defined cloud pressures and cloud fractions. The mean value of $V_{tropLNOx}$ (3.0 peta molec cm⁻²) is unchanged between v1.3 and v2.1_test. The increase in PE between v1.3 and 2.1_test is 14%–20% depending on background and profile option. LNO_x PE increases by ~60% when the 10th percentile $V_{tropbkgn}$ is substituted for a 30th percentile background. Therefore, improved estimates of $V_{tropbkgn}$ are essential for reducing uncertainties in PE (see section 5.2).

5.2. Analysis of Biases and Uncertainty

The standard deviation-based uncertainty of ~55% (mean of GLM16 and ENTLN coefficients of variation) is near the lower end of the formally determined uncertainty obtained by Allen et al. (2019) for a study using OMI NO₂ columns and WWLLN flashes. They obtained a high-bias and uncertainty of 20 ± 58%–73% after including a bias in AMF arising from biases in modeled NO/NO₂ ratios in the upper troposphere (Allen et al., 2019; Bucselo et al., 2019; Laughner & Cohen, 2017; Silvern et al., 2018) and summing in quadrature uncertainties in WWLLN DE (±25%–50% depending on DE value), tropospheric background (±30%), AMF_{LNOx} (20% ± 30%), NO_x lifetime (±25%) and several other minor error sources.

In this study as in Allen et al. (2019, 2021) and Bucselo et al. (2019), PE values are assumed to be biased high by 20% due to bases in AMF arising from positive biases in modeled NO/NO₂ ratios in the upper troposphere.

Allen et al. (2021) estimated LNO_x PE using NO₂ columns from GCAS and lightning counts from GLM16 and ENTLN. They obtained an overall uncertainty of 51.5% with major contributions from uncertainties in the areal extent of the enhanced LNO_x (±30%), DE (±21%), tropospheric background (±20%), and chemical lifetime of NO_x (±18%). These values can be compared to an earlier study by Allen et al. (2019) for the

Table 4
Sensitivity of v2.1_test LNO_x PE to Assumed Chemical Lifetime (τ), AMF, and Background option

NO _x τ (hours)	GLM16 (mol flash ⁻¹)	ENTLN (mol flash ⁻¹)
3	219 ± 124	150 ± 80
2	310 ± 195 (42%↑)	211 ± 133 (41%↑)
6	144 ± 82 (34%↓)	100 ± 51 (33%↓)
GMI AMF	191 ± 108 (13%↓)	130 ± 69 (13%↓)
Ott AMF	247 ± 139 (13% ↑)	170 ± 92 (13% ↑)
b10	268 ± 134 (22% ↑)	185 ± 96 (23% ↑)
b30	170 ± 114 (22%↓)	115 ± 65 (23%↓)
b00	267 ± 202 (22% ↑)	178 ± 150 (18% ↑)

Note: Percent changes in PE shown in parentheses are relative to mean GLM16 and ENTLN values for a three-hour chemical lifetime, mean of GMI and Ott AMFs, and mean of b10 and b30.

tropics using OMI NO₂ columns and WWLLN flashes that found an overall uncertainty of 58% with contributions from WWLLN DE ($\pm 25\%$ – 50%), chemical lifetime of upper tropospheric NO_x in the near-field of convection ($\pm 25\%$), and uncertainties in AMF_{LNO_x} associated with uncertainties in NO/NO₂ ratios ($+20\% \pm 30\%$). Similarly, Pickering et al. (2016) and Bucselo et al. (2019) found overall uncertainties of $\sim \pm 55\%$ for OMI/WWLLN studies centered over the Gulf of Mexico and Northern Hemisphere midlatitude continents, respectively.

In this study, we obtain an overall LNO_x PE uncertainty of 57% for optically detected GLM16 flashes and 56% for spheric-based ENTLN flashes. These values were obtained by summing the uncertainties in PE due to chemical lifetime (37.5%), tropospheric background (22.5%), advective loss (14%), AMF including NO/NO₂ ratios (30%), DE (10.5% for GLM16% and 3.5% for ENTLN), and other sources (10%) in quadrature. The uncertainty in PE due to chemical lifetime (37.5%) was obtained by comparing the PEs for τ equals 2 and 6 h with the PE for τ equals 3 h (see Table 4). Nault et al. (2016, 2017) give a range of 2–12 h for τ depending on the proximity to convection. A range of 2–6 h is used here because the PE evaluation is done using deep convective pixels in close proximity to the

lightning. The uncertainty in PE due to tropospheric background (22.5%) was obtained by comparing the PE for 10th percentile and 30th percentile backgrounds to the mean of the value for those backgrounds (Table 4). Justification for use of the 10th and 30th percentiles is given in the last paragraph of Section 3. The uncertainty associated with tropospheric background is higher in this study than in Allen et al. (2021) because the tropospheric columns from TROPOMI are of coarser spatial resolution than those from GCAS. The uncertainty associated with advective loss is assumed to be given by the coefficient of variation of the advective adjustment term shown in Table 2, which is 14%. The uncertainty in PE due to uncertainties in AMF including NO/NO₂ ratios is assumed to be 30%. See Section 4.3 of Allen et al. (2019) for justification. The uncertainty in PE due to DE is derived from the system-to-system variability in DE found during the GOES-R PLT field campaign. The normalized standard deviations during that campaign were 21% for GLM16% and 7% for ENTLN (see Table 2 of Allen et al., 2021). These are representative of the uncertainty in PE for individual case studies. The uncertainty of the mean PE is assumed to be 50% of the uncertainty in individual case studies or 10.5% for GLM16% and 3.5% for ENTLN. Biases and uncertainties in PE introduced by 20% day-night differences in GLM DE (Zhang & Cummins, 2020) were examined and determined to be minor. Specifically, the flash count was re-calculated for the 8 northwestern storms using a 70% nocturnal DE as opposed to the standard 50%. After adjusting for chemical decay assuming $\tau = 12$ h, the flash count decreased by an average of 4%. The uncertainty in PE due to other sources including systematic errors in slant columns, stratospheric vertical column amount, and optical cloud pressure (OCP) (Joiner et al., 2012) threshold is assumed to be 10%. Implicit in this low value is the assumption that a portion of these biases cancel when the tropospheric background is subtracted (Allen et al., 2019; Bucselo et al., 2019). The uncertainty in PE associated with flash-to-flash differences in flash channel length, flash energy, flash multiplicity, and flash altitude are not explicitly considered in this study; however, the dependence on PE on flash energy is discussed in section 5.3. The flash altitude is of interest because anomalous storms with a higher percentage of flashes occurring at high pressures (lower altitudes) may be more efficient at producing NO_x (Davis et al., 2019; Y. Wang et al., 1998). For simplicity, a bias and uncertainty of $+20 \pm 56\%$ will be used in this study regardless of flash source or characteristics. Applying these values to the GLM16 and ENTLN PEs shown in Table 3 results in final PEs of 175 ± 100 mol per flash for optical flashes based on GLM16 and 120 ± 65 mol per flash for spheric-based flashes from ENTLN.

Allen et al. (2021) obtained a considerably higher PE of 360 ± 180 mol per flash for GLM16 and 230 ± 115 mol per flash for ENTLN assuming τ equals 2 h and cancellation of biases.

However, their PE would be 230 ± 115 mol per flash for GLM16 and 150 ± 75 mol per flash for ENTLN if they also assumed 3 h for τ and a 20% high bias. These values are only $\sim 30\%$ higher than those obtained in this study. Therefore, much of the difference in PE between these studies could be an artifact of

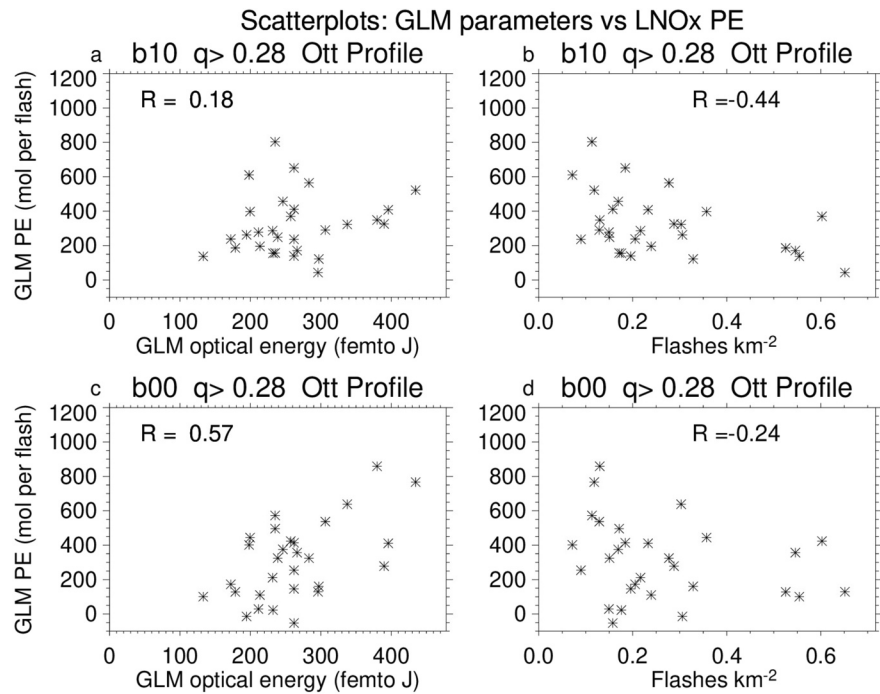


Figure 7. Scatterplots showing the relationship and correlation (R) between GLM16 flash products and GLM16-based nitrogen oxide produced by lightning (LNO_x) production efficiency (PE). (a) Optical energy (femto Joules) versus PE (mol per flash) for a 10th percentile tropospheric background, (b) Flash density (flashes km^{-2}) versus PE for a 10th percentile tropospheric background, (c) Optical energy versus PE assuming no tropospheric background, (b) Flash density versus PE assuming no tropospheric background.

assumptions. Thus, bottom-line PE values from satellite-derived studies of PE have limited value unless they are also accompanied by information on the assumptions used in deriving them. The uncertainty in these values is expected to be reduced with the launch of Tropospheric Emissions: Monitoring of Pollution (TEMPO) (Chance et al., 2019; Zoogman et al., 2017), which as of May 2021 is expected in fall 2022. For example, high temporal and spatial resolution observations from TEMPO will make it possible to use a Lagrangian approach to determine the chemical lifetime of NO_x in the near field of convection through an analysis of observed decreases in LNO_x -produced NO_2 columns with time. The uncertainty in PE due to chemical lifetime could be further reduced if additional measurements of NO_y species are available from TEMPO validation field campaigns. Until then, it will be difficult to reduce uncertainties in satellite-derived estimates of PE to less than 50%. This 50% uncertainty does not include systematic biases in PE due to differences in flash detection methodology between GLM and ENTLN.

5.3. Relation Between PE and Other Flash Metrics

The GCAS/GLM16 analysis (Allen et al., 2021) found that LNO_x PE was positively correlated with flash multiplicity ($r = 0.77$) and flash energy ($r = 0.83$) but negatively correlated with flash density ($r = -0.73$). Figure 7 shows scatterplots of GLM16 flash energy and GLM16 flash density versus TROPOMI/GLM PE for a 10th percentile background and for no background. As in the GCAS/GLM16 analysis, LNO_x PE is positively correlated with flash energy ($r = 0.57$ for no background and $r = 0.18$ for a 10th percentile background) and negative correlated with flash density ($r = -0.24$ for no background and $r = -0.44$ for a 10th percentile background); however, the correlations are weaker than were obtained during the GCAS analysis. The decrease in correlation after removal of the 10th percentile background suggests that a substantial number of the columns associated with the non-flashing pixels used in the determination of the background are affected by recent lightning- NO_x . Thus, PE estimates for individual case studies are highly uncertain. The negative correlation of PE with flash density is consistent with other studies that have shown that storms with higher flash densities have smaller individual flash channel lengths and produce less NO_x per flash.

However, it is not compelling support because a portion of the relatively small negative correlation is a consequence of the formulation of Equation 1, in which the PE is proportional to the area of the NO_x cloud divided by the flash total.

6. Conclusions

TROPOMI is a passive imaging spectrometer that retrieves NO_2 slant columns as well as cloud properties at horizontal resolutions as fine as 3.6 km (cross track) \times 5.6 km (along-track). Tropospheric column retrievals with TROPOMI are difficult over deep convective scenes due to saturation of Charged Coupled Device (CCD) pixels and blooming effects. However, tweaks to the processing algorithm between versions 1.2, 1.3, and 2.1_test allow more retrievals over these scenes and when coupled with a relaxation of the quality assurance threshold make it possible to estimate LNO_x PE for individual convective systems.

NO_x production per lightning flash was examined using retrievals from TROPOMI and flashes from GLM16 and ENTLN for 29 convective systems over the eastern- and central- United States and adjacent Gulf of Mexico and western Atlantic that occurred during the warm seasons of 2018 and 2019. GLM16 and ENTLN flash counts were adjusted for DE using mean DEs derived from a comparison with FECS. The resulting flash counts were compared for each of these systems. The analysis revealed that the DE for optical flashes was lower north of 40°N and west of 90°W. Thus, the GLM16 DE was reduced from 75% to 50% poleward of 40°N and west of 90°W. The lower DE for selected storms over the Upper Midwest and Great Plains suggests that these storms are more difficult to observe optically possibly because their anomalous charging structure results in lower flash heights.

For each of the 29 case studies, the moles of NO_x produced per flash was estimated using v2.1_test TROPOMI pixels with cloud fractions of greater than 0.95 and cloud pressures of less than 500 hPa, that is, deep convective pixels. The PE is calculated by multiplying the tropospheric column of NO_x due to recent lightning (V_{tropLNO_x}) by the storm area and dividing by the number of flashes (F) contributing to the column. F is a count of GLM16 or ENTLN flashes during the 12-h period preceding the time of the TROPOMI overpass. The count is adjusted for DE and advective loss and decayed exponentially to account for the relatively short NO_x lifetime in the vicinity of deep convection. V_{tropLNO_x} is equal to the median tropospheric column of NO_x over deep convective pixels (V_{tropNO_x}) minus a background representative of NO_x due to sources other than nonrecent lightning given by the 10th or 30th percentile of V_{tropNO_x} over pixels with no observed lightning. V_{tropNO_x} is obtained by dividing V_{tropNO_2} by a specially derived AMF that converts from NO_2 to NO_x using a priori profiles appropriate for a convective storm with lightning.

For the TROPOMI case studies, the mean PE for a three-hour chemical lifetime was determined to be 175 ± 100 mol per flash for optical flashes from GLM and 120 ± 65 mol per flash for radio-wave-detected flashes from ENTLN. These values include subtraction of a 20% high bias due to biases in modeled NO_2/NO_x ratios and include a 57% uncertainty due to uncertainties in chemical lifetime, tropospheric background, advective loss, AMF, and DE. GLM PE for individual systems was found to be positively correlated with optical energy ($r = 0.57$) before subtraction of the tropospheric background). Thus, approximately a third of the variability in PE between storms is related to variations in flash optical energy.

Appendix A: Analysis of TROPOMI products over deep convective scenes

In this study, the production of NO_x by lightning is examined using TROPOMI NO_2 columns over deep convective scenes, that is, pixels with cloud top pressures of less than 500 hPa and effective cloud fractions in the NO_2 window (f_{effNO_2}) (see Appendix C of van Geffen et al., 2019) ≥ 0.95 . The 0.95 threshold is applied to f_{effNO_2} instead of the radiative cloud fraction in the operational TROPOMI data product because the latter was found to have values of less than 0.95 within the centers of convective systems (see also Ludewig et al., 2020), as well as other anomalies. The f_{effNO_2} values are effectively empirical radiative cloud fractions derived from the geometrical cloud fraction, terrain reflectivity and viewing geometry, all of which are provided in the operational TROPOMI product.

Since mid-2018, we have investigated LNO_x PE using case studies over the United States. Our early analyses using versions 1.0, 1.1, and 1.2 of the TROPOMI product were hindered because vertical columns of NO_2

were not output for pixels with tropospheric AMFs less than 10% of the geometric AMF. This restriction did not affect the vast majority of pixels but did lead to data gaps over the pixels we are interested in, that is, pixels with low cloud top pressures and large cloud fractions. In order to facilitate our studies and studies by others, v1.3 of the TROPOMI product, which became operational in March 2019, includes vertical columns for these pixels resulting in much greater spatial coverage over deep convective systems.

Saturation of the TROPOMI detector in Band 4 used for the NO₂ retrievals and Band 6 used for FRESKO cloud retrievals is relatively common over bright clouds, that is, deep convective scenes with lightning, and can lead to missing cloud parameters and NO₂ columns (van Geffen et al., 2020). Saturation leads to one or more wavelength pixels in the radiance spectrum being flagged and omitted from the spectrum used to perform the SCD fit. However, SCD values in neighboring wavelength pixels may also spike due to the blooming effect as excess light spills over into adjacent wavelengths. To minimize the impact of these effects, v1.3 NO₂ retrievals are not performed if more than 1% of the radiance spectrum is flagged as saturated. To better deal with such spikes, the v2.0 NO₂ algorithm is equipped with a spike removal scheme that makes it possible to increase the saturation threshold and to obtain more usable retrievals over bright scenes (van Geffen et al., 2021). Specifically, wavelength pixels with fit residual values greater than a given threshold are marked as an outlier and not used in the Differential Atmospheric Absorption Spectroscopy (DOAS) fit. The number of outliers is tabulated, and retrievals are not performed when the number of outliers exceeds a threshold. The saturation and outlier thresholds vary with the versions of the L1B and NO₂ retrievals but are equal to 12% and 15 outliers for v2.1_test. The v2.1_test NO₂ retrievals used in this study include additional variables that are helpful for filtering. These variables include the number of outliers and an SCD quality flag that is set to 0 if no errors were reported during the retrieval and the SCD error is less than 2 petamolec cm⁻².

Each TROPOMI pixel includes a qa_value that can be used to filter the data. Each pixel begins with a qa_value of 1. This value is then multiplied by modification factors (f_{qa}^i) listed in Section E of the TROPOMI Algorithm Theoretical Basis Document (ATBD) for v2.2 of the tropospheric NO₂ product (van Geffen et al., 2021). Relevant modification factors include $f_{qa}^i = 0.74$ (cloud radiance fraction ≥ 0.5), $f_{qa}^i = 0.45$ ($AMF_{trop}/AMF_{geometric} < 0.1$), $f_{qa}^i = 0.15$ (SCD error > 2 petamolec cm⁻²), and $f_{qa}^i = 0.20$ (version 2 only: surface albedo in NO₂ window > 0.3). In this study, only \sim overcast scenes are considered, and AMF_{trop} and surface albedo are irrelevant. Therefore, we classify pixels with qa_values of 0.50–0.74 as “good quality”, pixels with qa_values of 0.28–0.49 as “fair quality”, and pixels with qa_values of 0.04–0.27 as “poor quality”. Table A1 shows the distribution of qa_values for v1.3 and v2.1_test TROPOMI pixels for the 29 case studies. Overall, there were 386,027 pixels within the various regions of interest. Of these pixels, 52,403 (13.6%) of v1.3 and 66,403 (17.2%) of v2.1_test pixels were classified as deep convective pixels. V2.1_test has 27% more deep convective pixels with slant columns than v1.3 due to a relaxation in the criteria used for cloud retrievals over bright scenes. The additional pixels include fair quality pixels, which increase by 36% and good-quality pixels, which increase by 22%. The increase in good-quality pixels is noteworthy because these pixels can be used without reservation for scientific studies over cloudy scenes. The number of fair-or-good quality pixels over flashing (non-flashing) pixels increased by 56% (25) between v1.3 and v2.1_test. Thus, lightning is a clear contributor to saturation/blooming and its impact on retrievals decreased between v1.3 and v2.1_test.

In this study, both good and fair quality pixels were used to estimate $V_{tropNOx}$. This restriction removes only a few pixels as the vast majority of pixels over deep convection are either good or fair in quality (see Table A1). Table A2 shows the mean and coefficient of variation (c_v) for S_{NO_2} , V_{tropNO_2} , and $V_{tropNOx}$ as a function of pixel

Table A1
Distribution of Quality Assurance Values and Percent of Flashing- and Non-flashing Pixels With Poor or Undefined Quality Retrievals

TROPOMI version	Total pixels	DC pixels	Good quality	Fair quality	Poor quality	No retrieval	Flashing $Q \geq 0.28$	No flash $Q \geq 0.28$
V1.3	386,027	52,403	27,710	24,025	336	332	5,696	46,039
v.2.1_test	386,027	66,403	33,675	32,654	69	5	8,882	57,447
%Change		+27	+22	+36	-79.5	-98.5	+56	+25

Table A2
Mean (peta molec cm^{-2}) and Coefficient of Variation (c_v) of S_{NO_2} , V_{tropNO_2} , and V_{tropNO_x} as a function of TROPOMI Version and qa_value Class

TROPOMI variable Version & qa_value class	S_{NO_2}		V_{tropNO_2}		V_{tropNO_x}	
	Mean	c_v	Mean	c_v	Mean	c_v
V1.3 good	9.42	0.21	4.78	1.24	6.83	1.09
V2.1_test good	9.41	0.22	4.76	1.21	7.08	1.10
V1.3 fair	9.50	0.18	59.2	3.53	6.73	0.87
V2.1_test_fair	9.38	0.17	22.7	1.35	6.65	0.86

quality and TROPOMI version. Mean values of S_{NO_2} vary little with TROPOMI version or retrieval quality. However, the story is more complicated for V_{tropNO_2} . For good quality pixels, the mean value of V_{tropNO_2} over deep convective pixels is nearly the same between v1.3 and v2.1_test. However, for fair-quality pixels, the mean value of V_{tropNO_2} decreases by nearly a factor of 3 from 59.2 to 22.7 petamolec cm^{-2} between v1.3 and v2.1_test. The coefficient of variation (c_v) is a metric useful for assessing the spatial heterogeneity of a data set with high values often an indicator of a noisy and/or unreliable data set. The c_v of V_{tropNO_2} associated with the fair-quality v1.3 retrievals (3.53) is much larger than that of the fair-quality v2.1_test retrievals (1.35) and good-quality retrievals (1.21–1.23). Thus, values of V_{tropNO_2} from fair-quality v1.3 pixels are noisy and should not be used. Values of V_{tropNO_2} over fair-quality v2.1_test pixels might be usable with care. In this study, V_{tropNO_2} is not needed to estimate V_{tropNO_x} and ultimately LNO_x PE. Instead, V_{tropNO_x} is determined using Equation 5 given in Section 3. Mean values of V_{tropNO_x} vary modestly with TROPOMI version and retrieval quality ranging from 6.65 to 7.08 petamolec cm^{-2} . The modest variability in V_{tropNO_x} and large variability in V_{tropNO_2} indicates that much of the variability in V_{tropNO_2} is caused by variability in AMF_{trop} , which is not used in Equation 5.

The relatively small difference in V_{tropNO_x} between good and fair pixels and the small value of c_v makes us comfortable using fair quality retrievals in our determination of V_{tropNO_x} . This is crucial for individual storms as the percent of deep convective pixels of good quality varies greatly from storm to storm (see Table 1) with three of the storms having 5% or fewer pixels of good quality. Thus, it is necessary to use both fair and good quality pixels to examine storm-to-storm variations in LNO_x PE. We note that all v2.1_test pixels of fair or good quality have SCD quality flags of 0 indicating that there are no known retrieval errors. The variability of c_v with outlier number was also examined and no dependence was found. Thus, all fair-quality pixels are used regardless of outlier number.

Finally, we had anticipated that V_{tropNO_x} would be higher over fair quality pixels than good quality pixels since fair quality pixels are more common in locations with flashes. However, this was not seen as the mean value of V_{tropNO_x} equaled 6.65 petamolec cm^{-2} over fair quality v2.1_test pixels and 7.08 petamolec cm^{-2} over good quality pixels.

Appendix B: Acronym list

A	area of deep convective storm
AdvL_i	advective loss of LNO_x
AMF	air mass factor
$\text{AMF}_{\text{LNO}_x}$	AMF used to convert tropospheric SCD of NO_2 to VCD of LNO_x
$\text{AMF}_{\text{strat}}$	stratospheric AMF from TROPOMI
AMF_{trop}	tropospheric AMF from TROPOMI
CCD	charged coupled device
CG	cloud-to-ground flashes
CH_4	methane
CRYSTAL-FACE	Cirrus Regional Study of Tropical Anvils and Cirrus Layers—Florida Area Cirrus Experiment

c_v	coefficient of variation equivalent to the normalized standard deviation
DC3	Deep Convective Clouds and Chemistry Field Experiment
DE	detection efficiency
DOAS	differential optical absorption spectroscopy
ENTLN	Earth Networks Total Lightning Network
F	flashes contributing to LNO _x column
f_{effNO_2}	effective cloud fraction in NO ₂ window
FAR	false alarm rate
FECS	Fly's Eye GLM Simulator
FRESKO	Fast Retrieval Scheme for Clouds from the Oxygen A-band
GCAS	NASA Goddard Geo-CAPE Airborne Simulator
Geo-CAPE	Geostationary Coastal and Air Pollution Events
GLM	Geostationary Lightning Mapper
GLM16	GLM on GOES-16
GLM17	GLM on GOES-17
GMI	Global Modeling Initiative
GMI AMF	AMF derived from profiles from the GMI model
GOES	Geostationary Operational Environmental Satellite(s)
GOES-R	GOES R-series
IC	intracloud or intercloud flashes
ISS-LIS	International Space Station-Lightning Imaging Sensor
LCFA	Lightning Cluster and Filtering Algorithm
LMA	Lightning Mapping Array
LNO _x	nitrogen oxides produced by lightning
MERRA-2	version 2 of the Modern-Era Retrospective analysis for Research and Applications
N_A	Avogadro's number
NO	nitric oxide
NO _x	nitrogen oxides
NO ₂	nitrogen dioxide
N ₂	molecular nitrogen
OCF	optical cloud pressure
OH	hydroxyl radical
OMI	Ozone Monitoring Instrument
Ott	AMF derived from cloud-scale simulations by Ott et al. (2010)
O ₂	molecular oxygen
O ₃	ozone
PE	production efficiency
GOES-R PLT	GOES-R Post Launch Test
qa_value	TROPOMI quality assurance value
SCD	slant column density
SNO ₂	SCD of NO ₂
TC4	Tropical Composition, Cloud and Climate Coupling
TEMPO	Tropospheric Emissions: Monitoring of Pollution
TROPOMI	Tropospheric Monitoring Instrument
t_o	time of TROPOMI overpass
t_i	time of individual flash
τ	chemical lifetime of LNO _x
UTC	Coordinated Universal Time
VCD	vertical column density
VNO ₂	tropospheric NO ₂ column
V_{tropbkgn}	vertical column of tropospheric NO _x due to non-recent lightning
V_{tropLNO_x}	vertical column of tropospheric NO _x due to recent lightning
V_{tropNO_x}	tropospheric column of NO _x
WWLLN	World Wide Lightning Location Network

Data Availability Statement

Data sets containing GLM16 flashes are accessible at https://www.avl.class.noaa.gov/saa/products/search?-datatype_family=GRGLM16PROD. V2.1_test TROPOMI NO₂ columns for each of the analyzed orbits are located at <https://doi.org/10.21944/tropomi-no2-inox-usa>. Data sets containing gridded files of AMF_{LNOx} for selected days including the dates of the 29 cases are located here: http://dsrs.atmos.umd.edu/DATA/allen_TROPOMI/. The latter directory also contains IDL code that can be used to read the text files. ENTLN data were obtained freely by request from Earth Networks (<https://www.earthnetworks.com>).

Acknowledgments

This research was funded under the NASA Aura Science Team (Principal Investigator, Nick Krotkov of NASA/Goddard).

References

- Allen, D. J., Pickering, K. E., Bucsel, E., Krotkov, N., & Holzworth, R. (2019). Lightning NO_x production in the tropics as determined using OMI NO₂ retrievals and WWLLN stroke data. *Journal of Geophysical Research: Atmospheres*, *124*(23), 13498–13518. <https://doi.org/10.1029/2018JD029824>
- Allen, D. J., Pickering, K. E., Duncan, B., & Damon, M. (2010). Impact of lightning NO emissions on North American photochemistry as determined using the global modeling initiative (GMI) model. *Journal of Geophysical Research*, *115*, D22301. <https://doi.org/10.1029/2010JD014062>
- Allen, D. J., Pickering, K. E., Lamsal, L., Mach, D. M., Quick, M. G., Lapierre, J., et al. (2021). Observations of lightning NO_x production from GOES-R post launch test field campaign flights. *Journal of Geophysical Research: Atmosphere*, *126*(8), e2020JD033769. <https://doi.org/10.1029/2020JD033769>
- Bateman, M., & Mach, D. (2020). Preliminary detection efficiency and false alarm rate assessment of the geostationary lightning mapper on the GOES-16 satellite. *Journal of Applied Remote Sensing*, *14*(3), 1. 032406. <https://doi.org/10.1117/1.JRS.14.032406>
- Bitzer, P. M. (2017). Global distribution and properties of continuing current in lightning. *Journal of Geophysical Research: Atmospheres*, *122*, 1033–1041. <https://doi.org/10.1002/2016JD025532>
- Blakeslee, R. J., Lang, T. J., Koshak, W. J., Buechler, D., Gatlin, P., Mach, D. M., et al. (2020). Three years of the lightning imaging sensor onboard the International Space Station: Expanded global coverage and enhanced applications. *Journal of Geophysical Research: Atmospheres*, *125*(16), e2020JD032918. <https://doi.org/10.1029/2020JD032918>
- Bruning, E. C., & MacGorman, D. R. (2013). Theory and observations of controls on lightning flash size spectra. *Journal of the Atmospheric Sciences*, *70*, 4012–4029. <https://doi.org/10.1175/jas-d-12-0289.1>
- Bruning, E. C., & Thomas, R. J. (2015). Lightning channel length and flash energy determined from moments of the flash area distribution. *Journal of Geophysical Research: Atmospheres*, *120*, 8925–8940. <https://doi.org/10.1002/2015JD023766>
- Bucsel, E. J., Pickering, K. E., Allen, D. J., Holzworth, R. H., & Krotkov, N. A. (2019). Midlatitude lightning NO_x Production efficiency inferred from OMI and WWLLN data. *Journal of Geophysical Research: Atmospheres*, *124*(23), 13475–13497. <https://doi.org/10.1029/2019JD030561>
- Bucsel, E. J., Pickering, K. E., Huntemann, T. L., Cohen, R. C., Perring, A., Gleason, J. F., et al. (2010). Lightning-generated NO_x seen by the ozone monitoring instrument during NASA's tropical composition, cloud and climate coupling experiment (TC⁴). *Journal of Geophysical Research*, *115*, D00J10. <https://doi.org/10.1029/2009JD013118>
- Chance, K., Liu, X., Miller, C. C., González Abad, G., Huang, G., Nowlan, C., et al. (2019). TEMPO green paper: Chemistry, physics, and meteorology experiments with the tropospheric emissions: Monitoring of pollution instrument. *Proceedings of the Society of Photo-Optical Instrumentation Engineers*, *11151*, Sensors, Systems, and Next-Generation Satellites XXIII, 111510B. <https://doi.org/10.1117/12.2534883>
- Davis, T. C., Rutledge, S. A., & Fuchs, B. R. (2019). Lightning location, NO_x production, and transport by anomalous and normal polarity thunderstorms. *Journal of Geophysical Research: Atmospheres*, *124*, 8722–8742. <https://doi.org/10.1029/2018JD029979>
- Eskes, H. J., van Geffen, J. H. G. M., Boersma, K. F., Eichmann, K.-U., Apituley, A., Pedergnana, M., et al. (2019). *S5P/TROPOMI Level-2 product user manual nitrogen dioxide*. Report S5P-KNMI-L2-0021-MA, Version 3.0.0, 27 March 2019. ESA. Retrieved from <http://www.TROPOMI.eu/documents/pum/>
- Finney, D. L., Doherty, R. M., Wild, O., Stevenson, D. S., MacKenzie, I. A., & Blyth, A. M. (2018). A projected decrease in lightning under climate change. *Nature Climate Change*, *8*(3), 210–213. <https://doi.org/10.1038/s41558-018-0072-6>
- Fuchs, B. R., & Rutledge, S. A. (2018). Investigation of lightning flash locations in isolated convection using LMA observations. *Journal of Geophysical Research: Atmospheres*, *123*, 6158–6174. <https://doi.org/10.1002/2017JD027569>
- Gelaro, R., McCarty, W., Suárez, M. J., Todling, R., Molod, A., Takacs, L., et al. (2017). The modern-era retrospective analysis for research and applications, version 2 (MERRA-2). *Journal of Climate*, *30*(14), 5419–5454. <https://doi.org/10.1175/jcli-d-16-0758.1>
- Goodman, S. J., Blakeslee, R. J., Koshak, W. J., Mach, D., Bailey, J., Buechler, D., et al. (2013). The GOES-R geostationary lightning mapper (GLM). *Atmospheric Research*, *125–126*, 34–49. <https://doi.org/10.1016/j.atmosres.2013.01.006>
- Goodman, S. J., Mach, D., Koshak, W., & Blakeslee, R. (2012). *GLM16 lightning cluster-filter algorithm theoretical basis document*. (p. 73). NOAA/NESDIS/Center for Satellite Applications and Research (STAR). Retrieved from <https://www.star.nesdis.noaa.gov/goesr/docs/ATBD/LCFA.pdf>
- Joiner, J., Vasilkov, A. P., Gupta, P., Bhartia, P. K., Veeckind, P., Sneep, M., et al. (2012). Fast simulators for satellite cloud optical centroid pressure retrievals; evaluation of OMI cloud retrievals. *Atmospheric Measurement Technique*, *5*, 529–545. <https://doi.org/10.5194/amt-5-529-2012>
- Koshak, W., Mach, D., Bateman, M., Armstrong, P., & Virts, K. (2018). *GOES-16 GLM16 Level 2 Data full validation data quality product performance guide for data users*. Retrieved from https://www.ncdc.noaa.gov/sites/default/files/attachments/GOES16_GLM16_Full-Validation_ProductPerformanceGuide.pdf
- Lacis, A. A., Wuebbles, D. J., & Logan, J. A. (1990). Radiative forcing of climate by changes in the vertical distribution of ozone. *Journal of Geophysical Research*, *95*, 9971–9981. <https://doi.org/10.1029/JD095iD07p09971>
- Laughner, J. L., & Cohen, R. C. (2017). Quantification of the effect of modeled lightning NO₂ on UV-visible air mass factors. *Atmospheric Measurement Technique*, *10*(11), 4403–4419. <https://doi.org/10.5194/amt-10-4403-2017>
- Liaskos, C. E., Allen, D. J., & Pickering, K. E. (2015). Sensitivity of tropical tropospheric composition to lightning NO_x production as determined by replay simulations with GEOS-5. *Journal of Geophysical Research: Atmospheres*, *120*(16), 8512–8534. <https://doi.org/10.1002/2014JD022987>

- Ludewig, A., Kleipool, Q., Bartstra, R., Landzaat, R., Leloux, J., Loots, E., et al. (2020). In-flight calibration results of the TROPOMI payload on board the Sentinel-5 Precursor satellite. *Atmospheric Measurement Technique*, *13*, 3561–3580. <https://doi.org/10.5194/amt-13-3561-2020>
- Mach, D. M. (2020). Geostationary lightning mapper clustering algorithm stability. *Journal of Geophysical Research: Atmospheres*, *125*(5), e2019JD031900. <https://doi.org/10.1029/2019JD031900>
- Marchand, M., Hilburn, K., & Miller, S. D. (2019). Geostationary lightning mapper and Earth networks lightning detection over the contiguous United States and dependence on flash characteristics. *Journal of Geophysical Research: Atmospheres*, *124*, 11552–11567. <https://doi.org/10.1029/2019JD031039>
- Mecikalski, R. M., Bain, A. L., & Carey, L. D. (2015). Radar and lightning observations of deep moist convection across Northern Alabama during DC3: 21 May 2012. *Monthly Weather Review*, *143*, 2774–2794. <https://doi.org/10.1175/MWR-D-14-00250.1>
- Nault, B. A., Garland, C., Wooldridge, P. J., Brune, W. H., Campuzano-Jost, P., Crouse, J. D., et al. (2016). Observational constraints on the oxidation of NO_x in the upper troposphere. *The Journal of Physical Chemistry A*, *120*(9), 1468–1478. <https://doi.org/10.1021/acs.jpca.5b07824>
- Nault, B. A., Laughner, J. L., Wooldridge, P. J., Crouse, J. D., Dibb, J., Diskin, G., et al. (2017). Lightning NO_x emissions: Reconciling measured and modeled estimates with updated NO_x chemistry. *Geophysical Research Letters*, *44*, 9479–9488. <https://doi.org/10.1002/2017gl074436>
- Ott, L. E., Pickering, K. E., Stenchikov, G. L., Allen, D. J., DeCaria, A. J., Ridley, B., et al. (2010). Production of lightning NO_x and its vertical distribution calculated from three-dimensional cloud-scale chemical transport model simulations. *Journal of Geophysical Research*, *115*, D04301. <https://doi.org/10.1029/2009JD011880>
- Padula, F., Goodman, S. J., Pearlman, A., & Cao, C. (2017). *GOES-R PLT field campaign data collection*. Huntsville, Alabama, U.S.A: from the NASA EOSDIS Global Hydrology Resource Center Distributed Active Archive Center. Retrieved from <http://ghrc.nsstc.nasa.gov/>; <https://doi.org/10.5067/GOESRPLT/DATA10110.1109/figarss.2017.8126955>
- Peterson, M. (2019). Research applications for the geostationary lightning mapper operational lightning flash data product. *Journal of Geophysical Research: Atmospheres*, *124*, 10205–10231. <https://doi.org/10.1029/2019JD031054>
- Pickering, K. E., Bucselo, E., Allen, D., Ring, A., Holzworth, R., & Krotkov, N. (2016). Estimates of lightning NO_x production based on OMI NO₂ observations over the Gulf of Mexico. *Journal of Geophysical Research: Atmospheres*, *121*, 8668–8691. <https://doi.org/10.1002/2015JD024179>
- Quick, M. G., Christian, H. J., Jr, Blakeslee, R. J., Stewart, M. F., Corredor, D., & Podgorny, S. (2017). *Fly's Eye GLM16 Simulator Preliminary Validation Analysis*, Fall Meeting 2017, abstract#AE33A-2512, 2017AGUFMAE33A2512Q. AGU.
- Ridley, B., Ott, L., Pickering, K., Emmons, L., Montzka, D., Weinheimer, A., et al. (2004). Florida thunderstorms: A faucet of reactive nitrogen to the upper troposphere. *Journal of Geophysical Research*, *109*, D17305. <https://doi.org/10.1029/2004JD004769>
- Rudlosky, S. D., Goodman, S. J., Virts, K. S., & Bruning, E. C. (2019). Initial geostationary lightning mapper observations. *Geophysical Research Letters*, *46*, 1097–1104. <https://doi.org/10.1029/2018GL081052>
- Rust, W. D., MacGorman, D. R., Bruning, E. C., Weiss, S. A., Krehbiel, P. R., Thomas, R. J., et al. (2004). Inverted-polarity electrical structures in thunderstorms in the Severe thunderstorm electrification and precipitation study (STEPS). *Atmospheric Research*, *76*, 247–271. <https://doi.org/10.1016/j.atmosres.2004.11.029>
- Rutledge, S. A., Hilburn, K. A., Clayton, A., Fuchs, B., & Miller, S. D. (2020). Evaluating geostationary lightning mapper flash rates within intense convective storms. *Journal of Geophysical Research: Atmospheres*, *125*, e2020JD032827. <https://doi.org/10.1029/2020JD032827>
- Silvern, R. F., Jacob, D. J., Travis, K. R., Sherwen, T., Evans, M. J., Cohen, R. C., et al. (2018). Observed NO/NO₂ ratios in the upper troposphere imply errors in NO-NO₂-O₃ cycling kinetics or an unaccounted NO_x reservoir. *Geophysical Research Letters*, *45*(9), 4466–4474. <https://doi.org/10.1029/2018GL077728>
- Sonnenfeld, R., Lapiere, J., Contreras Vidal, L., Zhu, Y., & Stock, M. (2021). Earth networks lightning network performance. *Earth and Space Science Open Archive*. <https://doi.org/10.1002/essoar.10505572.1>
- van Geffen, J. H. G. M., Boersma, K. F., Eskes, H., Sneep, M., ter Linden, M., Zara, M., & Veeffkind, J. P. (2020). S5P TROPOMI NO₂ slant column retrieval: Method, stability, uncertainties and comparisons with OMI. *Atmospheric Measurement Technique*, *13*(3), 1315–1335. <https://doi.org/10.5194/amt-13-1315-2020>
- van Geffen, J. H. G. M., Eskes, H. J., Boersma, K. F., van Geffen, J. H. G. M., Eskes, H. J., Boersma, K. F., et al. (2019). *TROPOMI ATBD of the total and tropospheric NO₂ data products*, Report S5P-KNMI-L2-0005-RP Issue 1.4.0. De Bilt, the Netherlands: KNMI.
- van Geffen, J. H. G. M., Eskes, H. J., Boersma, K. F., & Veeffkind, J. P. (2021). *TROPOMI ATBD of the total and tropospheric NO₂ data products*, Report S5P-1005 KNMI-L2-0005-RP Version 2.2.0. De Bilt, the Netherlands: KNMI. Retrieved from <http://www.tropomi.eu/documents/atbd/>
- Veeffkind, J. P., Aben, I., McMullan, K., Förster, H., De Vries, J., Otter, G., et al. (2012). TROPOMI on the ESA Sentinel-5 Precursor: A GMES mission for global observations of the atmospheric composition for climate, air quality and ozone layer applications. *Remote Sensing of Environment*, *120*, 70–83. <https://doi.org/10.1016/j.rse.2011.09.027>
- Wang, P., Stammes, P., van der A, R., Pinardi, G., & van Roozendael, M. (2008). FRESKO+: An improved O₂ A-band cloud retrieval algorithm for tropospheric trace gas retrievals. *Atmospheric Chemistry and Physics*, *8*, 6565–6576. <https://doi.org/10.5194/acp-8-6565-2008>
- Wang, W.-C., Zhuang, Y.-C., & Bojkov, R. D. (1993). Climate implications of observed changes in ozone vertical distributions at middle and high latitudes of the northern hemisphere. *Geophysical Research Letters*, *20*, 1567–1570. <https://doi.org/10.1029/93gl01318>
- Wang, Y., DeSilva, A. W., Goldenbaum, G. C., & Dickerson, R. R. (1998). Nitric oxide production by simulated lightning: Dependence on current, energy, and pressure. *Journal of Geophysical Research*, *103*(D15), 19149–19159. <https://doi.org/10.1029/98JD01356>
- Zel'dovich, Y. B., Sadovnikov, P. Y., & Frank-Kamenetskii, D. A. (1947). Oxidation of nitrogen in combustion, M. Shelef. *Trans. Academy of Sciences of USSR. Institute of Chemical Physics, Moscow-Leningrad*.
- Zhang, D., & Cummins, K. L. (2020). Time evolution of satellite-based optical properties in lightning flashes, and its impact on GLM flash detection. *Journal of Geophysical Research: Atmospheres*, *125*, e2019JD032024. Special Section: A New Era of Lightning Observations from Space. <https://doi.org/10.1029/2019JD032024>
- Zhu, Y., Rakov, V. A., Tran, M. D., Stock, M. G., Heckman, S., Liu, C., et al. (2017). Evaluation of ENTLN performance characteristics based on the ground truth natural and rocket-triggered lightning data acquired in Florida. *Journal of Geophysical Research: Atmospheres*, *122*(18), 9858–9866. <https://doi.org/10.1002/2017JD027270>
- Zoogman, P., Liu, X., Suleiman, R. M., Pennington, W. F., Flittner, D. E., Al-Saadi, J. A., et al. (2017). Tropospheric emissions: Monitoring of pollution (TEMPO). *Journal of Quantitative Spectroscopy and Radiative Transfer*, *186*, 17–39. <https://doi.org/10.1016/j.jqsrt.2016.05.008>